Intermediate-temperature dynamics of one-dimensional Heisenberg antiferromagnets

Chiranjeeb Buragohain and Subir Sachdev
Department of Physics, Yale University, P.O. Box 208120, New Haven, Connecticut 06520-8120
(Received 11 November 1998)

We present a general theory for the intermediate-temperature (T) properties of Heisenberg antiferromagnets of spin-S ions on p-leg ladders, valid for $2Sp$ even or odd. Following an earlier proposal for $2Sp$ even [Damle and Sachdev, Phys. Rev. B **57**, 8307 (1998)], we argue that an integrable, classical, continuum model of a fixed-length, three-vector applies over an intermediate-temperature range; this range becomes very wide for moderate and large values of $2Sp$. The coupling constants of the effective model are known exactly in terms of the energy gap above the ground state Δ (for $2Sp$ even), or a crossover scale T_0 (for $2Sp$ odd). Analytic and numeric results for dynamic and transport properties are obtained, including some exact results for the spin-wave damping. Numerous quantitative predictions for neutron scattering and NMR experiments are made. A general discussion on the nature of $T>0$ transport in integrable systems is also presented: an exact solution of a toy model proves that diffusion can exist in integrable systems, provided proper care is taken in approaching the thermodynamic limit. [S0163-1829(99)00714-6]

I. INTRODUCTION

One-dimensional Heisenberg antiferromagnets are strongly interacting quantum many-body systems for which a detailed quantitative confrontation between theory and experiment has been possible. A rather precise and parameter-free understanding of their low-temperature dynamic properties has emerged in a number of recent NMR experiments performed by Takigawa and collaborators.[1–4] These systems can therefore serve as useful springboards towards deciphering the behavior of interacting systems of greater complexity.

The past theoretical work on the dynamic properties of these quantum antiferromagnets has focused mainly on the universal behavior in the asymptotic low-temperature (T) regime $T\to 0$.[4,5–8] In the present paper we will extend the theory to a separate range of intermediate temperatures. We shall argue that under suitable conditions, to be described precisely below, this intermediate-temperature range can be quite wide, and is described by a continuum dynamical model quite different from that required for $T\to 0$. This intermediate-temperature dynamics was discussed briefly for a limited class of antiferromagnets in the last section of Ref. 4.

Our work will also connect with earlier investigations of the dynamics of classical lattice antiferromagnets (Refs. 9 and 10, and references therein). In a sense, our paper provides a bridge between the modern quantum dynamics and the classical studies of the 1970s. There is an overlapping window of validity for our theory and the classical investigation of Reiter and Sjölander,[10] and here our results are generally consistent with theirs, although there are some details that disagree. We will review this earlier work, in the context of our results, in Sec. V.

A large fraction of the experimental examples of one-dimensional Heisenberg antiferromagnets consist of p parallel, coupled chains of spin-S ions (for $p=1$ these are ordinary spin chains, while for $p>1$ these are commonly referred to as p-leg ladders). For all $T<T^{(1)}_{\rm max}$, where $T^{(1)}_{\rm max}$ will be defined shortly, these antiferromagnets are described by a universal quantum field theory: the one-dimensional O(3) nonlinear sigma model. This field theory has the quantum partition function (in units with $\hbar=k_B=1$, which we use throughout)

$$\mathcal{Z}_Q=\int \mathcal{D}\mathbf{n}(x,\tau)\,\delta(\mathbf{n}^2-1)\exp\left(-\int dx\int_0^{1/T} d\tau\,\mathcal{L}\right)$$

$$\mathcal{L}=\frac{1}{2cg}\left[\left(\frac{\partial\mathbf{n}}{\partial\tau}-i\mathbf{H}\times\mathbf{n}\right)^2+c^2\left(\frac{\partial\mathbf{n}}{\partial x}\right)^2\right]+\frac{i\theta}{4\pi}\mathbf{n}\cdot\left(\frac{\partial\mathbf{n}}{\partial x}\times\frac{\partial\mathbf{n}}{\partial\tau}\right). \tag{1.1}$$

Here $\mathbf{n}(x,\tau)$ is a three-component unit vector representing the orientation of the antiferromagnetic order parameter at spatial position x and imaginary time τ, c is a spin-wave velocity, and $\mathbf{H}$ is a uniform external magnetic field—we will be interested only in the linear response to $\mathbf{H}$. There are two dimensionless coupling constants in $\mathcal{L}$, θ, and g. The first, θ, is the coefficient of a topological term, and has the value $\theta=\pi$ for $2Sp$ an odd integer, and the spectrum of excitations above the ground state is then gapless. For $2Sp$ an even integer, $\theta=0$, and then there is gap to all excitations. The coupling g plays a role in determining the energy scale at which certain crossovers (to be discussed below) take place, but does not modify the physics otherwise. A straightforward semiclassical (large S) derivation shows that

$$g\approx\frac{2}{Sp}\left[1+\left(1-\frac{1}{p}\right)\frac{J_\perp}{J}\right]^{1/2}$$

$$c\approx 2JSa\left[1+\left(1-\frac{1}{p}\right)\frac{J_\perp}{J}\right]^{1/2}, \tag{1.2}$$

where J is the exchange constant along the legs of the ladder, $J_\perp$ is exchange on the rungs, and a is the lattice spacing along the legs; we have assumed here a model with only nearest-neighbor exchange, but the estimates $g\sim 1/Sp$ and $c\sim JSa$ hold far more generally. An important observation is

 ©1999 The American Physical Society

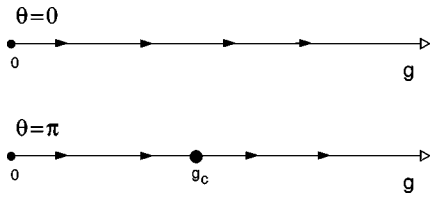

FIG. 1. Renormalization-group flows for the dimensionless coupling g in Eq. (1.1). For $\theta=0$,g has a runaway flow to $g=\infty$ and the ground state is a quantum paramagnet with a gap Δ. For $\theta=\pi$, there is a fixed point at $g=g_c$, of order unity, and near it the flow is $dg/d\ell \propto (g-g_c)^2$. This fixed point is described by the $k=1$,$SU(2)$ Wess-Zumino-Witten model. The crossover between the $g=0$ and $g=g_c$ fixed points takes place at an energy scale of order T_0. The region $g>g_c$ usually corresponds to a gapped state with spin-Peierls order, and is not considered in this paper.

that g becomes small for either large S or p. We will be especially interested in the small g case in this paper.

Let us now discuss the value of $T_{\max}^{(1)}$ below which Eq. (1.1) holds. The basic argument follows that made by Elstner *et al.*[11] in $d=2$. At a temperature T, the characteristic excited spin-wave has wavelength c/T, and the continuum quantum theory will apply as long as this wavelength is longer than the lattice spacing a of the underlying antiferromagnet. For p-leg ladders, description by a one-dimensional quantum model requires that the wavelength be larger than the width of the ladder, pa.[12] Using the value of c in Eq. (1.2), our estimate for $T_{\max}^{(1)}$ is then

$$T_{\max}^{(1)} \sim \frac{2JS}{p}\left[1+\left(1-\frac{1}{p}\right)\frac{J_\perp}{J}\right]^{1/2}. \tag{1.3}$$

To reiterate, the quantum theory (1.1) applies to the lattice antiferromagnet at all T below that in Eq. (1.3).

Let us now review the well-known, $T=0$, renormalization-group properties of Eq. (1.1).[13] The topological angle θ remains fixed at $\theta=0,\pi$, while the flows of the coupling g are sketched in Fig. 1.

For both cases $\theta=0,\pi$ there is a fixed point $g=0$ which is unstable at low energies. Indeed the beta function describing the flow away from $g=0$ is independent of θ to all orders in g. However, nonperturbative topological effects do distinguish the two values of θ. For $\theta=0$, the flow is believed to continue all the way to $g=\infty$, corresponding to a quantum paramagnetic ground state with an energy gap Δ. In contrast, for $\theta=\pi$, the flow is into a strong-coupling infrared stable fixed point at $g=g_c$. There is a scale-invariant and gapless theory which describes this fixed point—the $k=1$, $SU(2)$, Wess-Zumino-Witten model. For $g>g_c$, there is a runaway flow to $g=\infty$, usually associated with the appearance of spin-Peierls order; this last regime will not be discussed in this paper.

Our primary interest here shall be in the region in the vicinity of the unstable $g=0$ fixed point. For both $\theta=0,\pi$, there is a characteristic energy scale, usually denoted $\Lambda_{\overline{MS}}$, which determines the location of the crossover from the vicinity of the $g=0$ fixed point to the strong-coupling behavior. For energies or temperatures smaller than $\Lambda_{\overline{MS}}$, the strong-coupling behavior should apply, and as we have just discussed, this is quite different for $\theta=0$ and $\theta=\pi$. However, the physics at energies or temperatures larger than $\Lambda_{\overline{MS}}$ is controlled by the flow in the vicinity of the $g=0$ fixed point, and this is common to both $\theta=0$ and $\theta=\pi$. The energy scale $\Lambda_{\overline{MS}}$ can be estimated from the structure of the perturbative β function. For small g,

$$\Lambda_{\overline{MS}} \sim J \exp\left(-\frac{2\pi}{g}\right); \tag{1.4}$$

we have neglected here a prefactor of a power of g coming from higher-loop corrections. So from Eq. (1.2), for either S or p moderately large, the scale $\Lambda_{\overline{MS}}$ becomes *exponentially small.*

We are now ready to discuss the static thermodynamic properties of the quantum field theory (1.1) as a function of T. We will characterize the system by T dependence of two important observables: $\chi_u(T)$ and $\xi(T)$. The first is the uniform susceptibility χ_u, which is the linear response to the field $\mathbf{H}=(0,0,H)$: $\chi_u=(T/L)(d^2 \ln Z_Q/dH^2)|_{H=0}$, where L is the (infinite) length of the spatial direction; this is the susceptibility *per rung* of the ladder. The second is the correlation length $\xi(T)$, which determines the exponential decay of the equal-time two-point $\mathbf{n}$ field correlator as a function of x.

We will consider temperatures above and below $\Lambda_{\overline{MS}}$ in turn.

A. $T<\Lambda_{\overline{MS}}$

For $T<\Lambda_{\overline{MS}}$, as just noted, we must distinguish $\theta=0$ and $\theta=\pi$.

1. $\theta=0$

For $\theta=0$, there is an energy gap Δ, and the susceptibility is simply that of a dilute, thermally activated, classical gas of triplet magnons above the gap; these contribute an exponentially small susceptibility:[14,15]

$$\chi_u(T)=\left(\frac{2\Delta}{\pi T c^2}\right)^{1/2} e^{-\Delta/T}; \quad T<\Lambda_{\overline{MS}}, \quad \theta=0. \tag{1.5}$$

Experimentally, we can view Eq. (1.5) as the definition of the gap Δ and the velocity c, which are to be determined by fitting measurements to Eq. (1.5). The correlation length $\xi(T)$ takes a finite, T-independent value in this quantum paramagnet, up to correlations exponentially small in Δ/T; for the case where Δ is significantly smaller than J, we have[12,16]

$$\xi(T)=\frac{c}{\Delta}; \quad T<\Lambda_{\overline{MS}}, \quad \theta=0. \tag{1.6}$$

2. $\theta=\pi$

For the gapless case $\theta=\pi$, there are excitations with nonzero spin at arbitrarily low energies, and so $\chi_u(T)$ remains nonzero as $T\to 0$:[18,19]

$$\chi_u(T)=\frac{1}{2\pi c}\left(1+\frac{1}{2\ln(T_0/T)}-\frac{\ln[\ln(T_0/T)]}{4\ln^2(T_0/T)}+\cdots\right);$$
$$T<\Lambda_{\overline{MS}}, \quad \theta=\pi. \tag{1.7}$$

Again, this experimentally defines c and a temperature scale T_0 which determines the onset of a logarithmic correction to the $T=0$ susceptibility due to the slow flow into the fixed point at $g=g_c$. The correlation length of this critical paramagnet now diverges as $T\to 0$:[5–8,20]

$$\xi(T)=\frac{c}{\pi T}\left(1+\frac{1}{2\ln(T_0/T)}-\frac{\ln[\ln(T_0/T)]-1}{4\ln^2(T_0/T)}+\cdots\right);$$
$$T<\Lambda_{\overline{MS}},\quad \theta=\pi. \tag{1.8}$$

The dynamical properties of quantum antiferromagnets in the low-temperature regime $T<\Lambda_{\overline{MS}}$ have been discussed at length in Ref. 4 for the gapped case ($\theta=0$) and in Refs. 5–8 for the gapless case ($\theta=\pi$).

Note that both Δ and T_0 are energy scales characterizing the flow *into* the strong-coupling region. These should therefore be universally related to $\Lambda_{\overline{MS}}$ which is the scale of flows *out of* the weak-coupling region. We will discuss the universal relation shortly, once we have defined $\Lambda_{\overline{MS}}$ more precisely.

B. $T>\Lambda_{\overline{MS}}$

Let us now consider the regime $\Lambda_{\overline{MS}}<T<T^{(1)}_{\max}$; the upper bound is necessary to ensure that the continuum quantum theory still applies. The existence of this intermediate-temperature regime requires that $\Lambda_{\overline{MS}}<T^{(1)}_{\max}$, a condition that is not well satisfied for small S and p, and so this regime almost certainly does not exist for $p=1$ and $S=1/2,1$, but there is evidence that it is present for $p=1, S=2$.[17] Here we are controlled by physics in the vicinity of the $g=0$ fixed point, and it should be possible to treat quantum fluctuations in a renormalized perturbation theory in g. As discussed in Ref. 4, a nonperturbative treatment of the thermal fluctuations is still necessary, but this can be carried out exactly because of the low spatial dimensionality. The result of such a calculation is[4]

$$\chi_u(T)=\frac{1}{3\pi c}\left[\ln\left(\frac{4\pi e^{-1-\gamma}T}{\Lambda_{\overline{MS}}}\right)+\ln\ln\frac{T}{\Lambda_{\overline{MS}}}+\cdots\right];$$
$$\Lambda_{\overline{MS}}<T<T^{(1)}_{\max}, \tag{1.9}$$

where γ is Euler's constant. This result can also be viewed as the precise experimental definition of $\Lambda_{\overline{MS}}$. For completeness, we also quote the result in this regime for the correlation length $\xi(T)$:

$$\xi(T)=\frac{c}{2\pi T}\left[\ln\left(\frac{4\pi e^{-\gamma}T}{\Lambda_{\overline{MS}}}\right)+\ln\ln\frac{T}{\Lambda_{\overline{MS}}}+\cdots\right];$$
$$\Lambda_{\overline{MS}}<T<T^{(1)}_{\max}. \tag{1.10}$$

We now give the promised universal relationship between the energy scales characterizing the weak- ($\Lambda_{\overline{MS}}$) and strong- (Δ, T_0) coupling regimes. This requires nonperturbative knowledge of the renormalization-group flows, and can only be obtained from an analysis of the full thermodynamic Bethe-ansatz solution of the quantum field theory (1.1). For $\theta=0$, such an analysis was carried out in Ref. 21, and the result is now well known:

$$\Lambda_{\overline{MS}}=\frac{e}{8}\Delta;\quad \theta=0. \tag{1.11}$$

For the gapless case $\theta=\pi$, we will present a derivation of the required relationship in Appendix A, building upon some recent results;[22,23] our result is

$$\Lambda_{\overline{MS}}=\left(\frac{\pi}{2}\right)^{1/2}e^{3/4-\gamma}T_0;\quad \theta=\pi. \tag{1.12}$$

We are now finally in a position to state precisely the main objective of this paper. We will describe the dynamical properties of one-dimensional antiferromagnets in the intermediate-temperature regime $\Lambda_{\overline{MS}}<T<T^{(1)}_{\max}$. We quickly note as an aside that most of our results actually hold over a wider regime of temperatures $\Lambda_{\overline{MS}}<T<T^{(2)}_{\max}$, where we will define and discuss the origin of $T^{(2)}_{\max}>T^{(1)}_{\max}$ below; for now we ignore this point. A common treatment is possible for the $\theta=0$ and $\theta=\pi$ in this regime, with the two cases differing only in the input values of the static parameters $\chi_u(T)$ and $\xi(T)$ as defined by Eqs. (1.9)–(1.12). Moreover, as $\Lambda_{\overline{MS}}$ becomes exponentially small for moderate values of S or p, this regime can be quite wide and should be readily observable experimentally. Indeed, there is good evidence from recent measurements of static properties in quantum Monte Carlo simulations[17] that this universal intermediate-temperature regime exists even for $S=2$ spin chains.

The formulation of the dynamics properties for $\Lambda_{\overline{MS}}<T<T^{(1)}_{\max}$ was already discussed in Ref. 4. The key point[4] is to notice that the energy of a typical spin-wave excitation, which is of order $c\xi^{-1}(T)$, is parametrically smaller than T when ξ obeys Eq. (1.10). So the thermal occupation number of these spin-wave modes is large:

$$\frac{1}{e^{c\xi^{-1}/T}-1}\approx\frac{T}{c\xi^{-1}(T)}>1. \tag{1.13}$$

The second expression in Eq. (1.13) is the classical equipartition value, which indicates that the spin-wave excitations may be treated classically. The classical partition function controlling these fluctuations can be deduced by demanding that its correlations match with Eqs. (1.9) and (1.10), while the dynamic equation of motions follow by replacing the quantum commutators with Poisson brackets. In this manner, the problem reduces to the effective classical phase-space partition function[4]

$$\mathcal{Z}_C=\int\mathcal{D}\mathbf{n}(x)\mathcal{D}\mathbf{L}(x)\,\delta(\mathbf{n}^2-1)\,\delta(\mathbf{L}\cdot\mathbf{n})\exp\left(-\frac{\mathcal{H}_C}{T}\right),$$
$$\mathcal{H}_C=\frac{1}{2}\int dx\left[T\xi(T)\left(\frac{d\mathbf{n}}{dx}\right)^2+\frac{1}{\chi_{u\perp}(T)}\mathbf{L}^2\right]. \tag{1.14}$$

Here $\mathbf{n}(x)$ is a classical variable representing the orientation of the antiferromagnetic order and $\mathbf{L}(x)$ is its classical, canonically conjugate angular momentum. Because $\mathbf{n}(x)$ is of unit length, its motion is always in a direction orthogonal to its instantaneous direction, and there is no radial kinetic energy: the square of angular momentum represents the entire kinetic energy, and $\chi_{u\perp}$ is the moment of inertia of the fluc-

tuating **n**. The value of $\chi_{u,\perp}$ can be determined by realizing[4] that $\mathbf{L}(x)$ is simply the classical limit of the quantum operator corresponding to the magnetization density

$$\mathbf{L} = -\frac{\delta \mathcal{L}}{\delta H}; \tag{1.15}$$

then demanding that $\mathcal{Z}_C$ reproduce the correct uniform susceptibility to a uniform external field under which $\mathcal{H}_C \to \mathcal{H}_C - \int dx\, \mathbf{H}\cdot\mathbf{L}$, we obtain

$$\chi_u(T) = \frac{2}{3}\chi_{u\perp}(T); \tag{1.16}$$

the factor 2/3 comes from the constraint $\mathbf{L}\cdot\mathbf{n}=0$, so there are only two independent components of **L** at each spatial point.

Notice that Eq. (1.14) involves a functional integral over the commuting fields **n** and its conjugate momentum **L** as functions only of the spatial coordinate *x*, but is independent of the real time *t*. It therefore yields only equal-time correlation functions, as is the usual situation in classical statistical mechanics. To obtain unequal time correlators, we have to separately specify the equations of motion, and these are obtained by replacing quantum commutators with Poisson brackets. For the fields $\mathbf{n}(x), \mathbf{L}(x)$ these are

$$\{L_\alpha(x), L_\beta(x')\}_{PB} = \epsilon_{\alpha\beta\gamma} L_\gamma(x)\,\delta(x-x'),$$

$$\{L_\alpha(x), n_\beta(x')\}_{PB} = \epsilon_{\alpha\beta\gamma} n_\gamma(x)\,\delta(x-x'),$$

$$\{n_\alpha(x), n_\beta(x')\}_{PB} = 0, \tag{1.17}$$

where $\alpha,\beta,\gamma = 1,2,3$. The equations of motion (in real time) now follow from the Hamiltonian $\mathcal{H}_C$, and they are

$$\frac{\partial \mathbf{n}}{\partial t} = \frac{1}{\chi_{u\perp}(T)}\mathbf{L}\times\mathbf{n}$$

$$\frac{\partial \mathbf{L}}{\partial t} = [T\xi(T)]\mathbf{n}\times\frac{\partial^2 \mathbf{n}}{\partial x^2}. \tag{1.18}$$

We are now interested in unequal time correlation functions of Eq. (1.18), averaged over the classical ensemble of initial conditions specified by $\mathcal{Z}_C$.

To complete the quantum to classical mapping, we recall[4] the relationship between the correlations of the underlying antiferromagnet and the quantum field theory $\mathcal{Z}_Q$, and those of the classical nonlinear wave problem defined by Eqs. (1.14) and (1.18). Correlations of the antiferromagnet in the vicinity of the antiferromagnetic wave vector are given by the correlations of $\mathbf{n}(x,t)$ under $\mathcal{Z}_Q$, and are related to those in the classical problem by[4]

$$\langle \mathbf{n}(x,t)\cdot\mathbf{n}(0,0)\rangle_Q = \mathcal{A}\left[\ln\left(\frac{T}{\Lambda_{\overline{MS}}}\right)\right]^2 \langle \mathbf{n}(x,t)\cdot\mathbf{n}(0,0)\rangle_C, \tag{1.19}$$

where the subscript *Q* represents averages under the quantum partition function $\mathcal{Z}_Q$, the subscript *C* represents averages under the classical dynamical problem defined by Eqs. (1.14) and (1.18), and $\mathcal{A}$ is an overall *T*-independent normalization related to the amplitude of the correlations at $T=0$. Next, correlations of the antiferromagnet in the vicinity of zero wave vector are given by the correlations of $\mathbf{L}(x,t)$ under $\mathcal{Z}_Q$, and are essentially equal to those in the classical problem by[4]

$$\langle \mathbf{L}(x,t)\cdot\mathbf{L}(0,0)\rangle_Q = \langle \mathbf{L}(x,t)\cdot\mathbf{L}(0,0)\rangle_C. \tag{1.20}$$

The absence of an overall rescaling factor here is related to the conservation of the total magnetization density.

The main objective of this paper is to evaluate $\langle \mathbf{n}(x,t)\mathbf{n}(0,0)\rangle_C$ and $\langle \mathbf{L}(x,t)\mathbf{L}(0,0)\rangle_C$. An important property of these correlators is that they satisfy simple scaling laws which allow us to completely scale away all dependencies on $\xi(T)$ and $\chi_{u\perp}(T)$, and to express everything in terms of parameter-free universal functions. These scaling laws follow from the fact that Eqs. (1.14) and (1.18) define a continuum classical problem which is free of all ultraviolet divergences: this will become evident from our analytic computations in Sec. II and the numerical results of Sec. III. Consequently, simple engineering dimensional analysis involving rescaling of *x*, *t*, and **L** can be used to absorb dependences on the dimensionful parameters. In this manner, it is not difficult to show that[4]

$$\langle \mathbf{n}(x,t)\cdot\mathbf{n}(0,0)\rangle_C = \Phi_{\mathbf{n}}(\overline{x,t}),$$

$$\langle \mathbf{L}(x,t)\cdot\mathbf{L}(0,0)\rangle_C = \left(\frac{T\chi_{u\perp}(T)}{\xi(T)}\right)\Phi_{\mathbf{L}}(\overline{x,t}), \tag{1.21}$$

where

$$\overline{x} \equiv \frac{x}{\xi(T)},$$

$$\overline{t} \equiv t\left(\frac{T}{\xi(T)\chi_{u\perp}(T)}\right)^{1/2}, \tag{1.22}$$

and $\Phi_{\mathbf{n}}(\overline{x,t})$ and $\Phi_{\mathbf{L}}(\overline{x,t})$ are universal scaling functions. It is the primary task of this paper to determine these scaling functions. In principle, these scaling functions are determined by solving Eqs. (1.14) and (1.18) after setting all parameters equal to unity, $T=\xi=\chi_{u\perp}=1$, while replacing x,t by $\overline{x},\overline{t}$. Notice that the resulting equation is then parameter-free, and so there is no explicit small parameter in which any kind of expansion can be carried out; nothing short of an exact solution will do. We think this reasoning invalidates some of the conjectures on exactness of results made in Ref. 10, as we will discuss further in Sec. V. However, when the arguments of the scaling functions are themselves small, i.e., $|\overline{x}|, |\overline{t}| \ll 1$, then a systematic perturbation expansion is possible, and this will be presented in Sec. II.

We close this introductory discussion by returning to the issue of the maximum temperature up to which these results can be applied to lattice antiferromagnets. The appearance here of a classical spin model suggests that one should think about classical spin models obtained by starting directly from the lattice quantum spin model, without the use of the quantum field theory $\mathcal{Z}_Q$ as an intermediate step.[11] Such a classical description will only work for large *S*, and we can ask the question of when the resulting classical model can be described by a continuum classical theory, which will clearly be the one defined by Eqs. (1.14) and (1.18). The correlation

length of a classical spin antiferromagnet is of order JS^2pa/T, and a continuum description will work provided this is larger than the lattice spacing a and the width of a ladder system pa. This gives us the estimate[11]

$$T_{\max}^{(2)} \sim JS^2. \tag{1.23}$$

In the regime $T_{\max}^{(1)} < T < T_{\max}^{(2)}$, we can use a purely classical description of the spin model: its correlation length and uniform susceptibility will not be universal, but has to be computed for the specific model under consideration. For the model with only nearest-neighbor exchange, a standard computation on the classical antiferromagnet gives for the uniform susceptibility

$$\chi_u(T) = \frac{p}{6Ja}\left[1+\left(1-\frac{1}{p}\right)\frac{J_\perp}{J}\right]^{-1}; \quad T_{\max}^{(1)} < T < T_{\max}^{(2)}, \tag{1.24}$$

and for the correlation length

$$\xi(T) = \frac{JS^2pa}{T}; \quad T_{\max}^{(1)} < T < T_{\max}^{(2)}. \tag{1.25}$$

It is satisfying to note that there is a precise agreement between the results (1.9), (1.10) and (1.24), (1.25) at the common boundary of their respective regions of validity, $T \sim T_{\max}^{(1)}$: for the nearest-neighbor model under consideration we use the estimates for g and c in Eq. (1.2), and then using $\ln(T/\Lambda_{\overline{MS}}) \approx 2\pi/g$, we find the required agreement.

It appears useful to review the final status of the regimes of validity of the model studied here. The universal continuum classical model [Eqs. (1.14) and (1.18)] describes all one-dimensional Heisenberg antiferromagnets in the temperature regime $\Lambda_{\overline{MS}} < T < T_{\max}^{(2)}$; this regime is wide and well defined for moderately large values of S or p, and there is evidence that it exists already for $p=1, S=2$.[17] The complete definition of this classical dynamical model requires the input of the temperature-dependent static parameters $\xi(T)$ and $\chi_u(T)$. In the regime $\Lambda_{\overline{MS}} < T < T_{\max}^{(1)}$ these parameters are universally specified by Eqs. (1.9) and (1.10), with $\Lambda_{\overline{MS}}$ given by Eq. (1.11) for gapped spin chains ($\theta=0$) and by Eq. (1.12) for gapless spin chains ($\theta=\pi$). In the higher temperature regime $T_{\max}^{(1)} < T < T_{\max}^{(2)}$, these parameters are given by Eqs. (1.24) and (1.25) for the model with only nearest-neighbor exchange, and by related nonuniversal expressions for other antiferromagnets.

The following sections contain technical details towards the determination of the scaling functions $\Phi_{\mathbf{n}}$ and $\Phi_{\mathbf{L}}$ in Eq. (1.21), along with some theoretical analysis on the relationship between integrability and diffusion. We will begin in Sec. II by describing the analytical short-time expansion of the correlators $\Phi_{\mathbf{n}}$ and $\Phi_{\mathbf{L}}$. The long-time limit will then be studied numerically in Sec. III. The subsequent Sec. IV discusses issues which are somewhat peripheral to the main focus of this paper: the continuum equations of motion (1.18) are known to be integrable,[24] and this raises numerous fundamental questions on the nature of spin transport in integrable systems. These will be addressed in Sec. IV by the study of a simple integrable toy model whose spin correlators can be determined in close form. Further, we will see that these correlators have a striking similarity to those of Eq. (1.18). Readers interested primarily in spin chains can omit Sec. IV and skip ahead to Sec. V where we will describe the implications of our results for experiments.

II. SHORT-TIME EXPANSION

This section will determine the small t expansion of the scaling functions $\Phi_{\mathbf{n}}$ and $\Phi_{\mathbf{L}}$ in Eq. (1.21). Normally, there is a completely straightforward way of determining the short-time expansion of interacting systems[25]—it can be related, order by order, to equal-time correlators involving higher moments of the fields. However, this standard procedure does *not* work for the model [(1.14) and (1.18)] of interest here. This is because we are dealing with a continuum model with an infinite number of degrees of freedom, $\mathbf{n}(x), \mathbf{L}(x)$, present at arbitrary short-distance scales. If we naively generate the moment expansion, we find that the terms quickly acquire rather severe ultraviolet divergences.

A separate theoretical tool is necessary to generate the short-time expansion, and this shall be described here. We shall use an analog of the field-theoretic method known as chiral perturbation theory. As we shall see below, the expansion is actually in powers of $|t|$—this implies a nonanalyticity in the t dependence at $t=0$, which is in fact the reason for the ultraviolet divergences in the moment expansion. The latter method only gives an analytic expansion in t, by construction.

In this section, and in Appendix B, we will use units in which $T = \chi_{u\perp}(T) = 1$. However, we will retain explicit dependence on $\xi \equiv \xi(T)$. It turns out to be quite useful to keep track of powers of ξ. Indeed, our computations will be designed to generate an expansion of the correlators in powers of $1/\xi$, and this is *a posteriori* seen to be a short-time expansion. We will return to physical units in stating our final results.

We will therefore consider the problem of unequal time correlation functions of the nonlinear partial differential equations

$$\frac{\partial \mathbf{n}}{\partial t} = \mathbf{L} \times \mathbf{n},$$

$$\frac{\partial \mathbf{L}}{\partial t} = \xi \mathbf{n} \times \frac{\partial^2 \mathbf{n}}{\partial x^2} \tag{2.1}$$

when averaged over the ensemble of initial conditions defined by the partition function

$$\mathcal{Z}_C = \int \mathcal{D}\mathbf{n}(x)\mathcal{D}\mathbf{L}(x)\,\delta(\mathbf{n}^2-1)\,\delta(\mathbf{L}\cdot\mathbf{n}) \times \exp\left\{-\frac{1}{2}\int dx\left[\xi\left(\frac{d\mathbf{n}}{dx}\right)^2 + \mathbf{L}^2 - 2\xi m^2 n_z\right]\right\}. \tag{2.2}$$

The last term in the action represents a field of strength ξm^2 turned on in the z direction and serves as a regularization parameter for our perturbation expansion. At the end of our calculations we shall let $m \to 0$. From this partition function, one can immediately find the equal-time correlation functions to be

$$\langle \mathbf{L}(x,0)\cdot\mathbf{L}(0,0)\rangle = 2\,\delta(x),$$

$$\langle \mathbf{n}(x,0)\cdot\mathbf{n}(0,0)\rangle = e^{-|x|/\xi}; \tag{2.3}$$

the subscript C is implied on all averages in this section, unless stated otherwise.

We first construct our perturbation expansion in powers of $1/\xi$ for the equal-time problem specified by Eq. (2.2), and check that we do arrive at the correct correlation functions as specified in Eq. (2.3). The extension to the unequal time problem will then be straightforward. First, the constraints on the fields $\mathbf{n}$ and $\mathbf{L}$ are solved by introducing two complex scalar fields ϕ and ψ:

$$n_x = \frac{1}{\sqrt{2\xi}}(\phi+\phi^*),$$

$$n_y = \frac{1}{i\sqrt{2\xi}}(\phi-\phi^*),$$

$$n_z = \sqrt{1-2\phi\phi^*/\xi},$$

$$L_x = \frac{1}{\sqrt{2}}(\psi+\psi^*),$$

$$L_y = \frac{1}{i\sqrt{2}}(\psi-\psi^*),$$

$$L_z = -\frac{\phi\psi^*+\phi^*\psi}{\sqrt{\xi}\sqrt{1-2\phi\phi^*/\xi}}. \tag{2.4}$$

We introduce this decomposition to the functional integral (2.2) and expand the square roots in power series of $1/\xi$. In this manner, we arrive at an interacting field theory with an infinite number of interactions, with $1/\xi$ as the small coupling. However, to any particular order in perturbation theory in $1/\xi$, we only need to keep a finite set of interactions terms. We evaluate the correlation functions in real space using the ordinary machinery of diagrammatic perturbation theory. It is well known that such a perturbation expansion is plagued by infrared divergences. The decomposition (2.4) takes it for granted that the $\mathbf{n}$ field is ordered in the z direction and ϕ represents small spin-wave fluctuations around the ordered state. The infrared divergences are a signature of the fact that this assumption is wrong in one dimension. By introducing the external field ξm^2, we introduce long-range order into the system and thus regularize the divergences. The divergences show up as poles in $1/m$. But if we calculate the O(3) invariant correlation functions as in Eq. (2.3), we find that all poles cancel. Keeping this in mind, it is not difficult to show that the results of perturbation theory agree with Eq. (2.3) at every order. The details are to be found in Appendix B.

Once we have the correlation functions in the equal-time ensemble, we proceed to evaluate the unequal time correlation functions. To do that we again insert Eq. (2.4) into the equations of motion (2.1) and expand in powers of $1/\xi$ to get

$$\frac{\partial\psi}{\partial t} = i\xi^{1/2}\left[\frac{\partial^2\phi}{\partial x^2}+\frac{1}{\xi}\frac{\partial}{\partial x}\left(\phi^2\frac{\partial\phi^*}{\partial x}\right)+\cdots\right],$$

$$\frac{\partial\phi}{\partial t} = -i\xi^{1/2}\left[\psi+\frac{1}{\xi}(\phi^2\psi^*)+\cdots\right]. \tag{2.5}$$

Higher-order terms add further nonlinear interactions. We solve the initial value problem for each of the fields by an iterative strategy. First the free wave equation is solved and the solution is plugged back into the lowest-order nonlinear term to solve the problem to the first order. To evaluate the correlation functions, we just multiply the fields and carry out the average over initial conditions. The initial condition averages are, of course, known from the calculations described above. The technical details are relegated to Appendix B and here we only quote the results to one-loop order:

$$\left(\frac{\xi(T)}{T\chi_{u\perp}(T)}\right)\langle \mathbf{L}(x,t)\cdot\mathbf{L}(0,0)\rangle$$
$$= [\,\delta(\overline{x-t})+\delta(\overline{x+t})]\left(1-\frac{|\overline{t}|}{2}\right)$$
$$+\frac{1}{2}[\,\theta(\overline{x+t})-\theta(\overline{x-t})]+\mathcal{O}(\overline{x,t}), \tag{2.6}$$

$$\langle \mathbf{n}(x,t)\cdot\mathbf{n}(0,0)\rangle_C$$
$$= 1-\frac{1}{2}(|\overline{x+t}|+|\overline{x-t}|)$$
$$+\frac{1}{16}[3(\overline{x+t})^2+3(\overline{x-t})^2+2|\overline{x+t}||\overline{x-t}|]$$
$$+\mathcal{O}(\overline{x,t})^3, \tag{2.7}$$

where $\overline{x}$ and $\overline{t}$ are defined in Eq. (1.22), and the delta function in Eq. (2.6) is interpreted as $\mathcal{O}(\overline{x,t})^{-1}$.

In these results if we set $t=0$, we immediately recover the equal-time results (2.3) to the corresponding order in $1/\xi$. The structure of the correlation function (2.6) reflects the causal propagation of the conserved angular-momentum $\mathbf{L}$. The first term simply represents the free propagation of the angular-momentum density which is completely concentrated on the ''light cone.'' However, interactions to order $1/\xi$ do modify the free propagation and transfer the angular momentum density from the surface of the light cone to its interior. This is represented by the second term which is nonvanishing only inside the light cone. It can be checked that the spatial integral of Eq. (2.6) remains independent of t, as must be the case due to conservation of total angular momentum.

The result (2.7) has significant implications for the dynamic structure factor $S(k,\omega)$ of the antiferromagnetic order parameter:

$$S(k,\omega) = \int dx\,dt\langle \mathbf{n}(x,t)\cdot\mathbf{n}(0,0)\rangle_Q e^{-i(kx-\omega t)}. \tag{2.8}$$

First, we note that the result (1.19) and the scaling form (1.21) imply that the dynamic structure factor satisfies

$$S(k,\omega)=\left(\frac{\xi(T)\chi_{u\perp}(T)}{T}\right)^{1/2}S(k)\Phi_S(\bar{k},\bar{\omega}), \tag{2.9}$$

where $S(k)$ is the equal-time structure factor, which is known exactly (apart from the overall normalization $\mathcal{A}$):

$$S(k)=\int_{-\infty}^{\infty}\frac{d\omega}{2\pi}S(k,\omega)=\mathcal{A}\left[\ln\left(\frac{T}{\Lambda_{\overline{MS}}}\right)\right]^2\frac{2\xi(T)}{1+k^2\xi^2(T)}, \tag{2.10}$$

and Φ_S is a universal scaling function of

$$\bar{k}=k\xi(T),$$

$$\bar{\omega}=\omega\left(\frac{\xi(T)\chi_{u\perp}(T)}{T}\right)^{1/2}, \tag{2.11}$$

which describes the relaxation of the equal-time correlations. The prefactor in Eq. (2.9) has been chosen so that the frequency integral over Φ_S is normalized to unity for every $\bar{k}$

$$\int_{-\infty}^{\infty}\frac{d\bar{\omega}}{2\pi}\Phi_S(\bar{k},\bar{\omega})=1. \tag{2.12}$$

We will now show that, modulo some very mild assumptions, the result (2.7) exactly fixes the form of $\Phi_S(\bar{k},\bar{\omega})$ for $|\bar{k}|\gg 1$. In this short-distance regime, we are at distances shorter than the correlation length, and the system should look almost ordered. So we may expect that the spectrum consists of weakly damped spin waves, and this motivates the following ansatz for Φ_S in the regime $|\bar{k}|\gg 1$ and $|\bar{\omega}|\sim|\bar{k}|$:

$$\Phi_S(\bar{k},\bar{\omega})=\frac{\gamma(\bar{k})}{(\bar{\omega}-\bar{k})^2+\gamma^2(\bar{k})}+\frac{\gamma(\bar{k})}{(\bar{\omega}+\bar{k})^2+\gamma^2(\bar{k})}, \tag{2.13}$$

where $\gamma(\bar{k})$ is the unknown spin-wave damping parameter; we will shortly determine the large $\bar{k}$ limit of $\gamma(\bar{k})$. We now have to take the Fourier transform of Eqs. (2.9), (2.10), and (2.13), and compare the result with Eq. (2.7). In making this comparison, we should keep in mind that the large k,ω behavior of $S(k,\omega)$ can only determine the *nonanalytic terms* in the small x,t expansion. First, the integral over frequencies can be performed exactly for the form (2.13), and Eq. (2.9) implies

$$\langle\mathbf{n}(x,t)\cdot\mathbf{n}(0,0)\rangle_C=\int\frac{d\bar{k}}{\pi}\frac{e^{i\bar{k}\bar{x}-\gamma(\bar{k})|\bar{t}|}\cos(\bar{k}\bar{t})}{\bar{k}^2+1}+\cdots. \tag{2.14}$$

We reiterate that Eq. (2.13) is valid only for $|\bar{k}|\gg 1$, and so only the $1/\bar{k}^2$ contribution from the $(\bar{k}^2+1)$ denominator in Eq. (2.14) can be taken seriously. Also, we already have a nonanalytic $|\bar{t}|$ dependence in the exponential, and so we can expand this in powers of $|\bar{t}|$; in this manner we reduce Eq. (2.14) to

$$\langle\mathbf{n}(x,t)\cdot\mathbf{n}(0,0)\rangle_C=\frac{2}{\pi}\int_{k_1}^{\infty}d\bar{k}\frac{\cos(\bar{k}\bar{x})\cos(\bar{k}\bar{t})}{\bar{k}^2}-\frac{2|\bar{t}|}{\pi}\int_{k_2}^{\infty}d\bar{k}\frac{\gamma(\bar{k})\cos(\bar{k}\bar{x})\cos(\bar{k}\bar{t})}{\bar{k}^2}+\cdots, \tag{2.15}$$

where $k_{1,2}$ are some large positive constants, and we have assumed that γ is an even function of $\bar{k}$. The values of the integrals over $\bar{k}$ surely depend upon p and p', but the key observation is that the nonanalytic terms in $\bar{x}$ and $\bar{t}$ do not. This follows from the result

$$\int_{k_1}^{\infty}\frac{dk}{k^{\nu}}\cos(kx)=\frac{\pi|x|^{\nu-1}}{2\Gamma(\nu)\cos(\pi\nu/2)}+\cdots, \tag{2.16}$$

where all omitted terms can be written as a series in nonnegative, even integer powers of x (this allows an additive constant, independent of x). We now assume $\gamma(\bar{k}\to\infty)\sim\bar{k}^{\alpha}$, and then demand consistency between Eqs. (2.15) and (2.16) and the nonanalytic terms in Eq. (2.7). It is easy to see that we must have $\alpha=0$, and so $\gamma(\infty)$ is a constant. Further, the unknown additive constant associated with the second integral in Eq. (2.15) must be such that there is no single $|t|$ term in the correlator. Applying Eq. (2.16) to Eq. (2.15) with this understanding, we deduce that

$$\langle\mathbf{n}(x,t)\cdot\mathbf{n}(0,0)\rangle_C=\cdots-\frac{1}{2}(|\bar{x}+\bar{t}|+|\bar{x}-\bar{t}|)(1-\gamma(\infty)|\bar{t}|)+\cdots, \tag{2.17}$$

where all omitted terms are either analytic in $\bar{x}$ and $\bar{t}$, or involve subleading nonanalyticities. We should now compare Eq. (2.17) with Eq. (2.7) by matching only the nonanalytic terms in the vicinity of the light cone $\bar{x}=\pm\bar{t}$. In this latter region we can approximate $|\bar{x}+\bar{t}||\bar{x}-\bar{t}|$ in Eq. (2.7) by $2|\bar{t}||\bar{x}\pm\bar{t}|$—then the nonanalytic terms in Eqs. (2.17) and (2.7) match perfectly, and we obtain one of our important exact results

$$\gamma(\infty)=\frac{1}{2}. \tag{2.18}$$

Returning to physical units via Eq. (2.11), we conclude that the frequency $\Gamma(T)\equiv(\omega/\bar{\omega})\gamma(\infty)$, given by

$$\Gamma(T)=\frac{1}{2}\left(\frac{T}{\xi(T)\chi_{u\perp}(T)}\right)^{1/2}, \tag{2.19}$$

describes damping of spin waves for $|k|\xi(T)\gg 1$. We will discuss the experimental implications of this result in Sec. V.

Results for the spin-wave damping have been obtained earlier by Reiter and Sjölander,[10] in their studies of classical lattice antiferromagnets. If we insert the classical values (1.24) and (1.25) into Eq. (2.19), we obtain

$$\Gamma(T)=\frac{T}{Sp}\left[1+\left(1-\frac{1}{p}\right)\frac{J_{\perp}}{J}\right]^{1/2}, \tag{2.20}$$

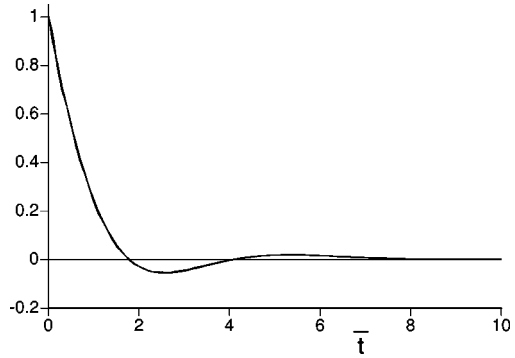

FIG. 2. The correlator $\langle \mathbf{n}(0,t)\cdot\mathbf{n}(0,0)\rangle_C$ as a function of $\overline{t}$, which is defined in Eq. (1.22). Results with lattice spacing $\xi/16$ and $\xi/8$ are shown, and their near perfect overlap indicates we have reached the continuum limit.

which agrees with their result for $p=1$. Keep in mind, though, that our result (2.19) has a much wider regime of applicability, beyond temperatures in which a purely classical thermodynamics holds. Further discussion on the relationship between our and earlier results appear in Sec. V.

III. NUMERICAL RESULTS

The previous section allowed us to determine the two-point correlators for small $|\overline{t}|$. Here we will present numerical simulations which examine the large $|\overline{t}|$ limit. These were performed on a discrete lattice realization of Eqs. (1.14) and (1.18), with lattice spacings of $\xi/16$ or larger, and had only nearest-neighbor couplings between the **n** vectors. Initial states were generated by thermalizing the system by the Wolff algorithm.[26] The time evolution was carried out by a fourth-order predictor-corrector method, and its accuracy was tested by keeping track of the conserved total energy and the lengths of the **n** vectors.

Our simulations are similar to many earlier studies of classical spin chains (see Refs. 27 and 28, and references therein). However, there is an important difference in that we are dealing with rotor variables **n** and **L**, rather than classical spins **S** which obey Poisson bracket relations like those for **L** in Eq. (1.17).

We will consider correlators of **n** and **L** in the following two subsections.

A. Correlations of n

We first consider dynamic correlators of **n**. The aim of our simulations is to obtain results for the dynamic structure factor $S(k,\omega)$ in regimes beyond the case $|\overline{k}|\gg 1$, $|\overline{\omega}|\sim|\overline{k}|$ which was studied by the short-time expansion. Our results were obtained for two cases—at equal positions (local) and at zero wave vector.

The local correlator is measured in NMR experiments, and we computed the local dynamic structure factor, $S_l(\omega)$, defined by

$$S_l(\omega)=\int_{-\infty}^{\infty} dt\langle \mathbf{n}(0,t)\cdot\mathbf{n}(0,0)\rangle_Q e^{i\omega t}=\int_{-\infty}^{\infty}\frac{dk}{2\pi}S(k,\omega). \tag{3.1}$$

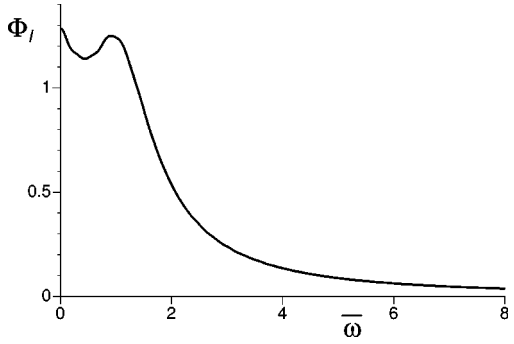

FIG. 3. The Fourier transform of Fig. 2 into frequency. This yields the universal scaling function Φ_l defined in Eq. (3.2).

By Eqs. (1.19) and (1.21), S_l satisfies the scaling form

$$S_l(\omega)=\mathcal{A}\left[\ln\left(\frac{T}{\Lambda_{\overline{MS}}}\right)\right]^2\left(\frac{\xi(T)\chi_{u\perp}(T)}{T}\right)^{1/2}\Phi_l(\overline{\omega}), \tag{3.2}$$

where Φ_l is a fully universal function (with no arbitrariness in its overall amplitude or the scale of its argument) with a unit integral over frequency

$$\int \frac{d\overline{\omega}}{2\pi}\Phi_l(\overline{\omega})=1. \tag{3.3}$$

Our results for the local time-dependent correlations are shown in Fig. 2 and its Fourier transform to frequency in Fig. 3. Two different lattice spacings were used, and the good overlap of the data confirms that we are examining the continuum limit. The correlations decay rapidly in time, but also show a brief, but clear oscillation; this oscillation results in a finite frequency peak in $S_l(\omega)$. We will discuss the physical origin of this oscillation after we have considered the zero-momentum correlator.

Turning to the zero-momentum correlator, we express our results in the scaling form (2.9) and obtain values for the scaling function $\Phi_S(0,\overline{\omega})$. We emphasize that the ansatz (2.13) does *not* hold for $\overline{k}=0$. Our results for the $k=0$ correlators of **n** are shown in the time domain in Fig. 4 and after the Fourier transform to frequency in Fig. 5.

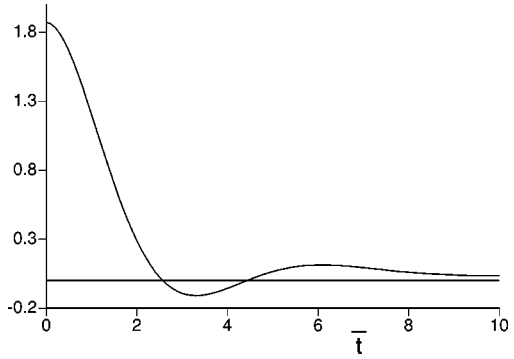

FIG. 4. The correlator $\int dx\langle \mathbf{n}(x,t)\cdot\mathbf{n}(0,0)\rangle_C/\xi(T)$ as a function of $\overline{t}$, which is defined in Eq. (1.22). We used a lattice spacing $\xi/8$. By Eq. (2.10), the $t=0$ value of this should be 2, and the difference is due to the finite lattice spacing.

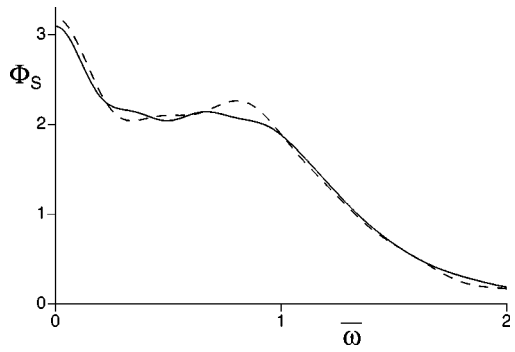

FIG. 5. The Fourier transform of Fig. 2 into frequency, which when combined with Eq. (2.9), leads to the universal scaling function $\Phi_S(0,\bar{\omega})$. The full line is at lattice spacing $\xi/8$, and the dashed line is for $\xi/16$. The data at $\xi/16$ is ''noisier'' because of insufficient averaging for the longer time data.

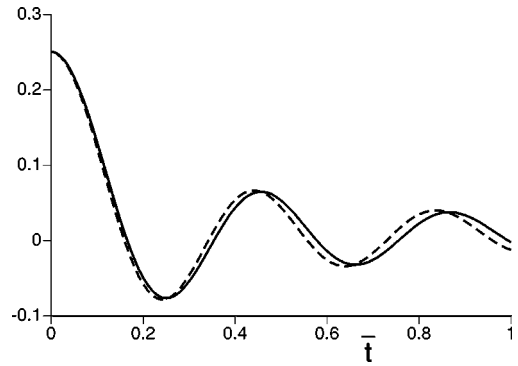

FIG. 6. Numerical results (full line) for the $[\xi(T)/T\chi_{u\perp}(T)]\times\langle \mathbf{L}(0,t)\cdot\mathbf{L}(0,0)\rangle$ correlation function for short times $\bar{t}<1$ on a lattice with spacing $\xi/8$. The results are compared with short time expansion (dashed line) in Eq. (3.6), valid for $\bar{t}\ll 1$.

As with the $x=0$ correlations above, the $k=0$ correlator shows a rapid decay, along with a brief oscillation; the latter leads to a finite frequency shoulder in $\Phi_S(0,\bar{\omega})$.

How do we understand this finite oscillation frequency observed in both the $x=0$ and $k=0$ correlators of $\mathbf{n}$? One way is to compare with the exactly known results[29,30] of the model with an N-component vector $\mathbf{n}$ in the limit of large N. At $N=\infty$, $S(0,\omega)$ consists of a delta function at a finite frequency $\omega\sim T/\ln(T/\Lambda_{\overline{MS}})$. So we can view the finite frequency as a remnant of the $N=\infty$ response at $N=3$. However, there is a related, more physical, way to interpret it. The underlying degrees of freedom have a fixed amplitude, with $|\mathbf{n}|=1$. However, correlations of $\mathbf{n}$ decay exponentially on a length scale $\xi(T)$—so if we imagine coarse graining out to $\xi(T)$, it is reasonable to expect significant *amplitude fluctuations* in the coarse-grained field, which we call ϕ_α. On a length scale of order $\xi(T)$, we expect the effective potential controlling fluctuations of ϕ_α to have a minimum at a nonzero value of $|\phi_\alpha|$, but to also allow fluctuations in $|\phi_\alpha|$ about this minimum. The finite frequency in Figs. 3 and 5 is due to the harmonic oscillations of ϕ_α about this potential minimum, while the dominant peak at $\omega=0$ is due to angular fluctuations along the zero energy contour in the effective potential. This interpretation is also consistent with the large N limit, in which we freely integrate over all components of $\mathbf{n}$, and so angular and amplitude fluctuations are not distinguished.

B. Correlations of L

We obtained numerical results only for the $x=0$ correlator of $\mathbf{L}$. The short-time behavior of this is given in Eq. (2.6). At long times, we expect the conservation of total $\mathbf{L}$ to be crucial in determining its asymptotic form. In particular, one natural assumption is that the long-time correlators of $\mathcal{L}$ are diffusive; in this case we expect

$$\langle \mathbf{L}(0,t)\cdot\mathbf{L}(0,0)\rangle = \frac{3T\chi_u}{(4\pi Dt)^{1/2}} \tag{3.4}$$

at large t. Consistency of this with the scaling form (1.21) implies that the diffusion constant D must obey

$$D=\mathcal{B}\frac{T^{1/2}[\xi(T)]^{3/2}}{[\chi_{u\perp}(T)]^{1/2}}, \tag{3.5}$$

where $\mathcal{B}$ is a dimensionless universal number.

Our numerical analysis of the autocorrelation was carried out on a system of 800 sites. The predictor-corrector method turns out to exactly conserve angular-momentum and we maintained energy conservation to four significant digits over the duration of the simulation. We averaged over 9600 initial conditions.

First we tested our results against the known exact short-time expansion. This is shown in Fig. 6. At these short times the lattice corrections are quite significant, and our comparison in Fig. 6 is with the chiral perturbation theory carried out in the presence of a lattice—the generalization of the result (2.6) to a lattice model with nearest-neighbor couplings and lattice spacing $\epsilon\xi$ is

$$\begin{aligned}\langle \mathbf{L}(x,t)\cdot\mathbf{L}(0,0)\rangle = 2\int_{-\pi/\epsilon}^{\pi/\epsilon}\frac{dk}{2\pi}e^{ik\bar{x}}\cos(\omega_k\bar{t})\\ \times\left(1+\int_{-\pi/\epsilon}^{\pi/\epsilon}\frac{dp}{2\pi}\frac{\cos(\omega_p\bar{t})e^{ip\bar{x}}-1}{\omega_p^2}\right)\\ +2\left(\int_{-\pi/\epsilon}^{\pi/\epsilon}\frac{dk}{2\pi}e^{ik\bar{x}}\sin(\omega_k\bar{t})\right)^2,\end{aligned} \tag{3.6}$$

where $\omega_k=\{2[1-\cos(\bar{k\epsilon})]/\epsilon^2\}^{1/2}$. It can be verified that Eq. (3.6) reduces to Eq. (2.6) in the limit $\epsilon\to 0$. As is clear from Fig. 6, the agreement between the analytical and numerical computations is quite satisfactory.

Finally, we turn to the numerical results at large $\bar{t}$. These are shown in Fig. 7. A best fit to the data with a power law $\bar{t}^{-\alpha}$ gave an optimum value of $\alpha=0.61$. However, an equally good fit to the data was obtained by the function $a_1/\sqrt{\bar{t}}+a_2/\bar{t}$, with the second subleading term contributing only about a 10% correction at the largest $\bar{t}$ (we found $a_2/a_1=0.65$). This second fit is consistent with diffusion—assuming this is the correct form, we obtain the estimate for the numerical prefactor in Eq. (3.5):

$$\mathcal{B}\approx 3.32. \tag{3.7}$$

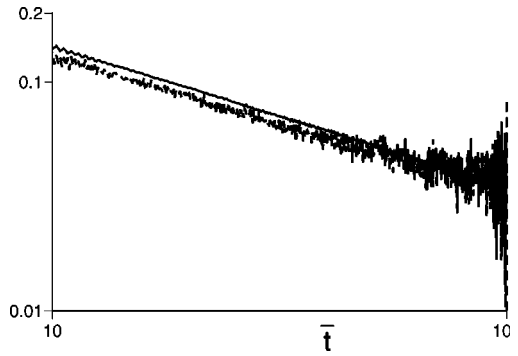

FIG. 7. Numerical results for $[\xi(T)/T\chi_{u\perp}(T)] \times\langle \mathbf{L}(0,t)\cdot\mathbf{L}(0,0)\rangle$ as a function of $\bar{t}$ in a log-log plot. The smoother line is for lattice spacing $\xi/8$, while the noisier line is for lattice spacing $\xi/16$. The agreement of the two results is evidence that this decay is a property of the continuum limit. A straight-line fit (not shown) to the $\xi/8$ data is almost perfect, and its slope indicates that the correlator decays as $\bar{t}^{-0.61}$. An equally good fit to the data was obtained by the function $a_1/\sqrt{\bar{t}}+a_2/\bar{t}$, with the second subleading term contributing only about a 10% correction at the largest $\bar{t}$.

In their studies of the classical lattice model, Reiter and Sjölander,[10] also computed the spin diffusivity. Diffusion is a property of the $|\bar{k}|\ll 1$ regime, and we do not expect their perturbative techniques to be exactly valid. Combining the classical values of $\chi_u(T),\xi(T)$, in Eqs. (1.24) and (1.25) with Eq. (3.5), their result translates into the value $\mathcal{B}=1$. This value is clearly inconsistent with our numerical result above.

IV. INTEGRABILITY AND DIFFUSION

This section will examine an integrable toy model of spin transport; readers interested mainly in the experimental implications of our results so far can move ahead to Sec. V. Others, not interested in the details of the toy model, may want to jump to Sec. IV C where we will discuss general implications of the toy model solution on spin transport in integrable systems.

The toy model we shall introduce is a variant of an effective model, considered in Ref. 4, for the dynamics in the regime $T<\Delta$ for gapped chains. Here, our strategy will be to introduce the model as worthy of study in its own right, as it is simple enough to allow determination of the spin-density correlator in closed form at all times. In the long-time limit, the correlator has a diffusive form, and so this example *proves* that there is no general incompatibility between integrability and diffusion. Further motivations in examining this model are the following:

(i) We shall show that the short-time behavior of the toy model is very similar to our result (2.6) for the continuum wave model [(1.14) and (1.18)]. This is suggestive, and indicates that the long-time diffusive behavior in Eq. (3.4) is not an unreasonable postulate.

(ii) The correlators of the integrable toy model can also be studied for the case of finite system of size L with periodic boundary conditions. This allows us to carefully examine the interplay of the limits $t\to\infty$ and $L\to\infty$. The diffusive form only appears if the $L\to\infty$ is taken first. In the opposite order of limits we find recurrent behavior with a great deal of structure dependent upon the microscopic details of the model. We think this issue of the orders of limit of $t\to\infty$ and $L\to\infty$ is of considerable relevance to recent studies of $T>0$ transport in integrable systems,[31–35] and this will be discussed further in Sec. IV C.

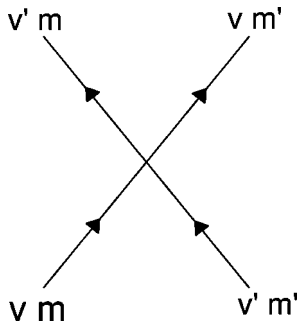

FIG. 8. Collision of two particles. They initially have velocities v,v' and spins m,m'. After the collision they exchange velocities but retain their spin.

We begin by describing the toy model. Place N point particles of equal mass at positions x_i $(i=0,1,\ldots N-1)$ which are chosen independently from a uniform distribution on a circle of length L. Now independently give each particle a velocity v_i, drawn from some distribution $g(v)$, and a ''spin'' m_i, drawn from some distribution $h(m)$. As the system evolves, the particles will move in straight trajectories, transporting their spin along with them. This will happen until two particles collide, and we now have to describe the nature of such collisions. We will restrict the collisions to satisfy the important constraints of conservation of total energy, momentum, and spin in each collision. The first two are already sufficient to determine the fate of the velocities (see Fig. 8): if we consistently label the particles from left to right (i.e., as we move around the circle counterclockwise, we always encounter the particles in the order $x_0,x_1,x_2,\ldots,x_{N-1}$), then the particles will simply exchange velocities in each collision.

In other words, in a collision between particle i and particle $i+1$, the velocity of the particle i after the collision is that of particle $i+1$ before the collision, and vice versa. How about the fate of the spins m_i and m_{i+1}? In principle, we can choose numerous possibilities interpolating between zero and total reflection, consistent with conservation of total spin $\Sigma_i m_i$. The exactly solvable models are the two extremes: zero or total reflection. The case of zero reflection is rather trivial and leads only to simple ballistic transport of spin along straight lines. We will therefore consider only the case of total reflection here: in the convention we are following of labeling the particles here, this corresponds to the statement that each m_i is a constant of the motion (see Fig. 8). So to summarize: in each collision the particles exchange velocities but their spins ''bounce off'' each other. We note that, although no exact solution is known, we expect the long-time correlations of a model with only partial reflection to be quite similar to that of the total reflection case, but with renormalized transport coefficients.

We shall be interested here in computing the correlators of the ''spin'' density $L(x,t)$, defined by

$$L(x,t)=\sum_{i=0}^{N-1} m_i \delta[x-x_i(t)], \tag{4.1}$$

where $x_i(t)$ are the positions of the particles: these consist of piecewise straight lines which reflect at each collision. We shall compute the two-point correlator of $L(x,t)$, averaged over the ensemble of initial conditions defined above. Further, we will choose our distributions $g(v)$ and $h(m)$ to be even, i.e., on the average, the total net momentum and spin are zero. Then, because the initial momenta and spin are uncorrelated, we have

$$\begin{aligned}\langle L(x,t)L(0,0)\rangle &= \sum_{i,i'} \langle m_i m_{i'}\rangle \langle \delta[x-x_i(t)]\delta[x_{i'}(0)]\rangle \\ &= \langle m^2\rangle \sum_i \langle \delta[x-x_i(t)]\delta[x_i(0)]\rangle \\ &= \langle m^2\rangle \rho P(x,t),\end{aligned} \tag{4.2}$$

where $P(x,t)$ is the probability that a particle at $x=0$ at time $t=0$ is at the position x at time t,

$$\langle m^2\rangle = \sum_m m^2 h(m), \tag{4.3}$$

and $\rho=N/L$ is the density of particles.

Most of our results will be on a particular simple velocity distribution, which is designed to mimic the properties of the continuum model [(1.14) and (1.18)]:

$$g(v)=\frac{1}{2}[\delta(v-c)+\delta(v+c)]. \tag{4.4}$$

So each particle is allowed to have only one of two velocities $\pm c$. This is similar to the fact that linear spin waves in the continuum wave model also have velocities $\pm c$.

The remainder of this section will describe the computation of the function $P(x,t)$ using the method of Jepsen.[36] Although later more elegant solutions were put forward by Lebowitz and Percus[37] for solving the model in the thermodynamic limit, we shall use the relatively cumbersome machinery of Jepsen because it allows us to consider finite systems.

At time $t=0$ the N particles are at random positions on the ring. We shall put the origin of the coordinate system at the location of particle 0. The rest of the particles from $0,1,2,\ldots,N-1$ are numbered such that the $(i+1)$th particle is immediately to the right of the ith one. As a particle moves with uniform velocity, in a ''space-time'' diagram we can represent its motion as a straight line which will call a trajectory. When two trajectories cross, there is a collision. The particles bounce off each other, and in effect the particles exchange trajectories. So at the beginning the zeroth particle starts on the zeroth trajectory and as this trajectory crosses others, the zeroth particle moves onto a different trajectory.

Now define $A_{jk}(t)$ to be one if the particle j is on the trajectory k at time t and zero otherwise. If we form an ensemble of systems, the average $\langle A_{jk}(t)\rangle$ is the probability that the particle j is on the trajectory k at time t. A knowledge of $A_{jk}(t)$ for all values of j,k,t constitutes a full solution to the dynamics of the system. The solution is defined by[36]

$$A_{jk}(t)=\frac{1}{N}\sum_u e^{-iju}\prod_{h=0}^{N-1} S[u,w_{kh}],$$

$$u=\frac{2\pi l}{N}, \quad l=0,1,2,\ldots,N-1; \quad \sum_u \equiv \sum_{l=0}^{N-1},$$

$$S[u,w]=e^{inu} \text{ when } (n-1)L<w\leqslant nL \text{ for each } n,$$

$$w_{kh}=x_k-x_h+(v_k-v_h)t. \tag{4.5}$$

We shall note some periodicity properties of $S[u,w]$ and $A_{jk}(t)$ here. By the above definition

$$S[u,w+L]=e^{iu}S[u,w], \text{ hence } S[u,w+NL]=S[u,w]. \tag{4.6}$$

Also, for the distribution (4.4), noting the fact that $|v_k-v_h|=0,2c$, we arrive at

$$\begin{aligned}A_{jk}\left(t+\frac{NL}{2c}\right) &= \frac{1}{N}\sum_u e^{-iju}\prod_{h=0}^{N-1} S\left(u,w_{kh}+NL\frac{v_k-v_h}{2c}\right) \\ &= A_{jk}(t).\end{aligned} \tag{4.7}$$

Let us define a time $\mathcal{T}\equiv L/c$ which is the time required by a free particle to go once around the system. Every trajectory returns exactly to its starting point after this interval of time. It is now obvious that in a period of time $NL/c=N\mathcal{T}$, each particle will return to its initial positions and velocities. Thus the Poincaré recurrence time of the system, with the velocities chosen under Eq. (4.4), is of order N, rather than being of the order of e^N or larger.

A. Diffusion in the thermodynamic limit

Now we go to the thermodynamic limit and address the question of diffusion. The limit is defined such that N and L approach infinity while the density $N/L=\rho$ is held finite. The zero particle starts out at the origin and we ask what is the probability, $P(y,t)$, that it is at position y at time t (both y and t are held finite as the limit $L\to\infty$ is taken). This can be written as

$$P(y,t)=\langle \delta[y-x_0(t)]\rangle = \sum_k \langle \delta(y-x_k-v_k t)A_{0k}(t)\rangle, \tag{4.8}$$

where the angular brackets are an average over all possible initial ensembles of velocity and positions of particles, while keeping the zero particle at the origin. The average can be evaluated exactly, and there is a simple, closed-form result:

$$\begin{aligned}P(y,t) &= \frac{1}{2}[\delta(y+ct)+\delta(y-ct)]e^{-\rho c|t|}+\frac{\rho}{2}[\theta(y+ct) \\ &\quad -\theta(y-ct)]e^{-\rho c|t|}\left(\frac{c|t|}{\sqrt{c^2t^2-y^2}}I_1(\rho\sqrt{c^2t^2-y^2})\right. \\ &\quad \left.+I_0(\rho\sqrt{c^2t^2-y^2})\right).\end{aligned} \tag{4.9}$$

I_0 and I_1 are the modified Bessel functions of order zero and one, respectively. The resemblance to the correlation func-

tion of the nonlinear wave model given in Eq. (2.6) is clear. The first term in Eq. (4.9) is a delta function along the light cone, but its contribution decreases exponentially with time. The second term lies within the light cone, and becomes increasingly important for large time. Also, if we take the short time limit of Eq. (4.9), we get

$$P(y,t)=\frac{1}{2}[\delta(y+ct)+\delta(y-ct)](1-\rho c|t|+\cdots)$$

$$+\frac{\rho}{2}[\theta(y+ct)-\theta(y-ct)], \tag{4.10}$$

which is precisely of the form (2.6). However, unlike Eq. (2.6), we can now also study the long-time limit analytically. We take this limit within the light cone with $y\sim\sqrt{t}$, and then the asymptotic expansions of the modified Bessel functions yields

$$P(y)\approx\frac{1}{(4\pi Dt)^{1/2}}\exp\left(-\frac{y^2}{4Dt}\right), \tag{4.11}$$

$$D=\frac{c}{2\rho}, \tag{4.12}$$

which is the diffusive form assumed for the classical wave model in Eq. (3.4). As shown by Jepsen, this calculation can also be done for a general velocity distribution $g(v)$, and provided the distribution is symmetric in v, we obtain Eq. (4.12) but with

$$D=\frac{1}{\rho}\int_0^\infty v g(v)dv. \tag{4.13}$$

B. Effect of periodic boundary conditions in a finite geometry

Here we go back to the finite system and think more about it. The fact that the Poincaré recurrence time is only linear in N, is because of the fact that the phase space becomes very restricted once we allow only two possible velocities. An interesting effect is that the recurrence time can be very different depending upon whether there are an even or odd number of particles in the system. The recurrence time is the lowest common multiple of $\mathcal{T}$ (the time required for trajectories to return to their initial position) and $NL/2c=N\mathcal{T}/2$ (the time required for particles to come back to their initial trajectory). With an odd number of particles, $N=2p-1$, the recurrence time is $N\mathcal{T}=(2p-1)\mathcal{T}$ as mentioned above. But if we add one single extra particle to the system, the recurrence time almost becomes half because $NL/2c=N\mathcal{T}/2=p\mathcal{T}$ is an exact multiple of $\mathcal{T}$.

In fact, the recurrence time could be even smaller. If we take an even number N of particles and choose their velocities as $\pm c$ randomly, the most likely scenario is one where half of them have velocity $+c$, and the rest have velocities $-c$. In that case,

$$A_{jk}(t+\mathcal{T})=\frac{1}{N}\sum_u e^{-iju}\prod_{h=0}^{N-1} S[u,w_{kh}+\mathcal{T}(v_k-v_h)]. \tag{4.14}$$

Amongst all the factors that we have in the product on the right-hand-side (RHS), half of them will not contribute any phase to the product because for them $v_k-v_h=0$. The other half will contribute a phase of exactly $\exp(\pm 2iu)$ each. So the total phase contribution will be $\exp(\pm 2iuN/2)\equiv 1$. Hence the most probable recurrence time for a random ensemble of even number of particles is $\mathcal{T}$. It turns out that with reflecting hard wall boundary conditions, the recurrence time is $2\mathcal{T}$ regardless of the initial conditions.

Now let us see how the effect of the recurrence time might show up in the probability distribution of a diffusing particle. We shall essentially try to find the autocorrelation function for a single specific particle moving around in a ring for all times $t<\mathcal{T}=L/c$ and $t>\mathcal{T}=L/c$. We shall again choose this particle to be the zero particle and at time $t=0$, its position and velocity are $x_0\equiv 0$ and v_0, respectively. The probability distribution is defined as before in Eq. (4.8). Since $A_{jk}(t)$ is periodic with a period of $N\mathcal{T}/2$, all distribution functions will also be periodic with the same period. Moreover,

$$\begin{aligned}A_{jk}(N\mathcal{T}/2-t)&=\frac{1}{N}\sum_u e^{-iju}\\ &\quad\times\prod_{h=0}^{N-1} S[u,w_{kh}+(v_k-v_h)(N\mathcal{T}/2-t)]\\ &=\frac{1}{N}\sum_u e^{-iju}\prod_{h=0}^{N-1} S[u,w_{kh}-(v_k-v_h)t].\end{aligned} \tag{4.15}$$

When we carry out the average over the initial conditions, the particles k and h will have the velocities $+v_k,+v_h$ and $-v_k,-v_h$ with equal probability. So the probability distribution function will satisfy

$$P(y,N\mathcal{T}/2-t)=P(y,t). \tag{4.16}$$

Thus we need to evaluate this function only for $0\leqslant t\leqslant N\mathcal{T}/4$.

The details of the evaluation of $P(y,t)$ are again relegated to the appendix. Let us represent the distribution function as

$$\begin{aligned}P(y,t)&=[\delta(y+ct)+\delta(y-ct)]P^{(1)}(t)\\ &\quad+[\theta(y+ct)-\theta(y-ct)]P^{(2)}(y,t).\end{aligned} \tag{4.17}$$

We write down explicit series solutions for $P^{(1)}(t)$ and $P^{(2)}(0,t)$. These sums could not be evaluated in a closed analytic form. So we carried out the sums numerically for specific values of N and L. $P^{(1)}(t)$ and $P^{(2)}(0,t)$ are plotted in Figs. 9 and 10, respectively.

For times $t\ll\mathcal{T}$ and $N\gg 1$ with N/L fixed, these results reduce to the results (4.9) derived in the thermodynamic limit. For $t>\mathcal{T}$, we see lots of complicated structures. Not all of them are well understood. But some of the prominent ones are easy to understand. For example at times $t=n\mathcal{T}$, $n=1,2,3,\ldots$, we see peaks in $P^{(1)}$, each of whose height turns out to be $1/\sqrt{2\pi N}$. The origin of this is very easy to understand. Out of the whole ensemble of initial conditions, a fraction of them will have exactly half of the particles with velocity $+c$ and the others with velocity $-c$ (with the as-

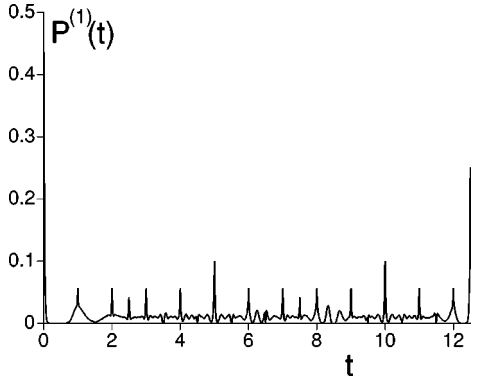

FIG. 9. The probability distribution function $P^{(1)}(t)$ plotted as a function of time $0 \leqslant t \leqslant N\mathcal{T}/4$ for $N=50$. The unit of time is $\mathcal{T}$. The stronger peaks at multiples of five are due to the fact that five is a prime factor of N.

sumption that N is even). Since these sets of initial conditions have a recurrence time of only $\mathcal{T}$, so they come back to the original distribution after a time $\mathcal{T}$ and hence contribute to this peak. Using the binomial distribution, it is easy to prove that the fraction of ensembles which have exactly half the particles with one velocity and the other half with the opposite velocity is exactly $\sqrt{2/\pi N}$. The extra factor of 1/2 comes from the fact that we have both left- and right-going initial conditions for our test particle. If we change the number of particles by one, N becomes odd. So no set of initial conditions will have a recurrence time $\mathcal{T}$, and these peaks will disappear as shown in Fig. 11.

C. Discussion

Our study of an integrable toy model in this section has highlighted the extreme importance of taking the limits of long time $t \to \infty$, and large system size $L \to \infty$ with proper care. If we send $L \to \infty$ *first*, then we explicitly demonstrated the existence of spin diffusion in the subsequent long-time limit. This is, of course, the correct thermodynamic limit, and the presence of spin diffusion also makes physical sense. Once the limit $L \to \infty$ has been taken, an infinite number of parameters are needed to specify the initial thermal state of the system; diffusion then arises when some local degree of freedom starts to sample an increasing number of these infinite number of random initial conditions with the passage of time.

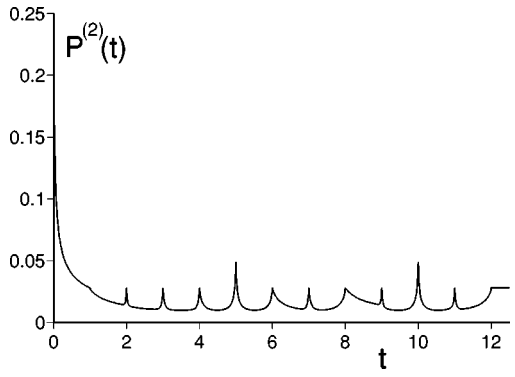

FIG. 10. The probability distribution function $P^{(2)}(t)$ plotted as a function of time for $N=50$ for $0<t<N\mathcal{T}/4$. The unit of time is $\mathcal{T}$.

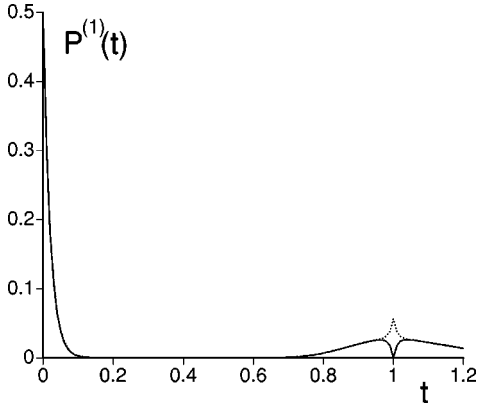

FIG. 11. The probability distribution function $P^{(1)}(t)$ plotted as a function of time for $N=50$ (dashed line) and $N=51$ (full line). The unit of time is $\mathcal{T}$. Notice the disappearance of the peak at $t=1$ for $N=51$.

On the other hand, very different results were obtained for the limit $t \to \infty$ at any fixed L. Here the integrable nature of the system was immediately evident, and we observed a bizarre set of recurrences dependent sensitively on details of the microscopic Hamiltonian. The Poincaré recurrence time of our toy model was quite short, and this was clearly due to its integrability. No sign of spin diffusion was seen.

A number of recent studies have examined the issue of $T>0$ spin transport in integrable quantum systems.[31–35] A model of particular interest has been the $S=1/2$ XXZ chain. At the $SU(2)$ symmetric point (the XXX chain), the low-T properties of this antiferromagnet are expected to be in the universality class of $\mathcal{L}$ in Eq. (1.1) at $\theta=\pi$. So studies of the XXX model will explicate the nature of spin transport at temperatures $T<T_0$ at $\theta=\pi$. This is a regime for which our paper has no results (although, spin transport in the low $T<\Delta$ regime for $\theta=0$ was studied in Ref. 4). However, we have examined the higher temperature regime $T_0<T<T^{(2)}_{\max}$ in Sec. III B, and found that our numerical results are not inconsistent with the presence of spin diffusion. It would then seem natural that diffusion may also exist for $T<T_0$, although this is, of course, not a rigorous argument. The latest numerical evidence for the XXX chain[33,35] seems to be consistent with the existence of diffusion.

Here we wish to issue a small caution towards the method used to study transport in Refs. 31–33 and 35 (this caution does not apply to Ref. 34). These works computed a ''stiffness,'' which is the coefficient of zero-frequency delta function in the frequency dependent conductivity. By its very construction, such a quantity is defined at $\omega=0$ in a finite system; so implicitly, the limit $\omega \to 0$ has been taken before the $L \to \infty$ limit. The considerations of this section make it amply clear that such a procedure is potentially dangerous.

V. IMPLICATIONS FOR EXPERIMENTS

First, we summarize the main theoretical results of this paper. We have shown that there is an intermediate-temperature range over which the static and dynamic properties of a large class of one-dimensional Heisenberg antiferromagnets are described by the deterministic, continuum model defined by Eqs. (1.14) and (1.18). For p-leg ladders of

spin-S ions, this temperature range rapidly becomes quite wide as Sp increases. For $2Sp$ even, our universal results hold for $\Delta < T < T^{(2)}_{\max}$, where Δ is the ground-state energy gap, and $T^{(2)}_{\max}$ is estimated in Eq. (1.23), while for $2Sp$ odd, they hold for $T_0 < T < T^{(2)}_{\max}$, where T_0 is an energy scale measuring the strength of logarithmic corrections at the lowest T. Both T_0 and Δ become exponentially small as Sp increases, and so the intermediate-temperature regime is clearly defined. The dynamical properties of such antiferromagnets are encapsulated in the scaling forms (1.21), which relate them to universal functions dependent only upon two thermodynamic parameters: the antiferromagnetic correlation length $\xi(T)$, and the uniform spin susceptibility $\chi_u(T)$. We obtained information on the universal functions in Secs. II and III, including exact results on the spin-wave damping, while exact results for $\xi(T)$ and $\chi_u(T)$ were presented in Sec. I.

We now briefly review the work in the 1970s on the dynamics of classical antiferromagnetic chain (Refs. 9 and 10 and references therein). As we saw in Sec. I, there is a window of temperatures $T^{(1)}_{\max} < T < T^{(2)}_{\max}$ [$T^{(1)}_{\max}$ was estimated in Eq. (1.3)], over which Eqs. (1.24) and (1.25) are valid, where our results apply to purely classical models; so there is a common regime of validity between our and earlier work. These earlier classical results were all obtained on studies of lattice antiferromagnets, and all used some variant of the short-time moment expansion to extrapolate to the long-time limit by a physically motivated ansatz, e.g., the memory function formalism; however, there is a degree of arbitrariness in any such ansatz. In a regime where their correlation length $\xi \gg a$ (where a is a lattice spacing), and the wave vectors $ka \ll 1$, their results should be described by the continuum model we have discussed here. However, we expect their short-time methods to be exact only for $k\xi \gg 1$. Indeed, our paper provides a proper description of the scaling structure, along with quantitative information on the scaling functions, in the nonperturbative regime $k\xi \ll 1$. Consistent with these expectations, we saw in Sec. II that our result (2.20) for the spin-wave damping for $k\xi \gg 1$, and $T^{(1)}_{\max} < T < T^{(2)}_{\max}$, was in precise agreement with that of Reiter and Sjölander.[10] It should be noted, however, that our result (2.19) for the damping remains exact over a much wider window of temperatures ($T_0, \Delta < T < T^{(2)}_{\max}$), including when χ_u and ξ have the quantum renormalized T dependence in Eqs. (1.9) and (1.10). Moreover, we believe, despite conjectures by Reiter and Sjölander to the contrary, that the results in Ref. 10 are not exact for $k\xi \ll 1$—we saw in Sec. III B that our value for the spin-diffusion constant (assuming the existence of diffusion) D disagreed with theirs.

Turning to experiments, single chain ($p=1$) antiferromagnets with $S>1$ which have been studied are $(CD_3)_4NMnCl_3$ (TMMC) (Refs. 38 and 39) which has $S=5/2$, $(C_{10}H_8N_2)MnCl_3$ (Ref. 40) which has $S=2$, and $CsVCl_3$ (Ref. 41) which has $S=3/2$. We think it would be worthwhile to reexamine these materials from a modern perspective, given the numerous exact results that are now available.

Among static properties, neutron-scattering experiments[38] have measured the correlation length $\xi(T)$, and these have been compared to purely classical theories in which $\xi(T)$ behaves like Eq. (1.25). At lower temperatures, $\xi(T)$ should exhibit the logarithmic temperature dependence in Eq. (1.10), arising from quantum fluctuations. Combined with measurements of the uniform susceptibility $\chi_u(T)$, a rather precise test of the quantum-renormalized static theory should then be possible.

Dynamic tests of the theory have focused mainly on the linewidth of the spin-wave excitations in the regime $k\xi \gg 1$. The measured linewidths have been compared[39,41] with the prediction of the classical theory,[10] which yields the result (2.20). This is in general agreement with the theory, but a quantitative discrepancy was observed[41] for $S=3/2$. We think it would be useful to compare the experiments with our exact result (2.19), while using the actual experimentally observed values of ξ and χ_u.

We think future neutron-scattering experiments should also examine the interesting regime $k\xi \ll 1$. Here we have provided numerically exact results in Sec. III. In particular, there is some interesting physics in the structure of the frequency-dependent lineshapes in Figs. 3 and 5, and these should be subjected to experimental tests. Also, we can easily generate additional universal spectra at other positions in the energy-momentum space, as needed.

The results in Sec. III also provide quantitative predictions for NMR experiments on spin chains. The nuclear relaxation rate $1/T_1$ is given by local low-frequency dynamic structure factor of the electronic spins. This has two contributions, one from the ferromagnetic component given by the correlator of $\mathbf{L}$, and the other from the antiferromagnetic component given by the correlator of $\mathbf{n}$. Let us parametrize the electronic spin $\mathbf{S}_i$ by

$$\mathbf{S}_i = (-1)^i S \mathbf{n}(x_i) + \frac{a}{p} \mathbf{L}(x_i), \tag{5.1}$$

where a is the lattice spacing. If we assume that

$$\frac{1}{T_1} = \frac{\Gamma}{2} \int_{-\infty}^{\infty} dt\, e^{i\omega_N t} \langle [S_{xi}(t) + iS_{yi}(t)][S_{xi}(0) - iS_{yi}(0)] \rangle, \tag{5.2}$$

where Γ is related to the hyperfine coupling, and $\omega_N \to 0$ is the nuclear Larmor frequency. The electron-spin correlator has to be evaluated in the presence of an applied magnetic field H, and the electron Larmor precession can usually be neglected. However, for the case where there is spin diffusion, as in the assumed form (3.4), then this electron precession must be included for the Fourier transform is divergent at low frequencies. Combining Eqs. (5.1) and (5.2) with the results of Sec. III, we obtain

$$\frac{1}{T_1} = \Gamma \left\{ \frac{\mathcal{A} S^2}{3} \left[\ln\left(\frac{T}{\Lambda_{\overline{MS}}} \right) \right]^2 \left(\frac{\xi(T) \chi_{u\perp}(T)}{T} \right)^{1/2} \Phi_l(0) + \frac{T \chi_u(T) (a/p)^2}{\sqrt{2DH}} \right\}, \tag{5.3}$$

where D is estimated in Eqs. (3.5) and (3.7). If we ignore logarithmic factors, the first antiferromagnetic term in Eq. (5.3) is of order Γ/T while the second ferromagnetic term is of order $(\Gamma/T)(Ta/c)^2 (T/H)^{1/2}$; either term could be domi-

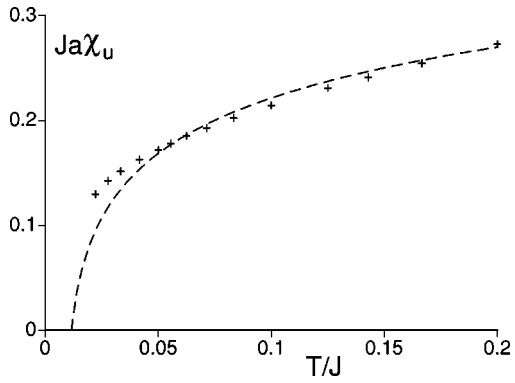

FIG. 12. Comparison of the numerical results of Ref. 42 (plus marks) for the uniform susceptibility χ_u of a five-leg ladder with $S=1/2$ with the theoretical predictions of Eqs. (1.9) and (1.12) (dashed line). All exchange constants are nearest neighbor and have magnitude J, and the lattice spacing is a. The value of χ_u is *per rung.*

nant, depending upon the magnitude of H. Further, our result (5.3) has assumed the existence of spin diffusion, but we expect that Eq. (5.3) will provide a reasonable quantitative estimate of the H and T dependence for experimental purposes, even if this assumption is not entirely correct in its details: there is clearly a long-time tail in Fig. 7, even if it is not precisely diffusive.

Finally, we compare our theoretical predictions with quantum Monte Carlo simulations on odd-leg ladders. Numerical results for $\chi_u(T)$ have been obtained recently by Frischmuth *et al.*[42] on antiferromagnets with $S=1/2$ and $p=3,5$. We compared their results for $p=5$ with our result [Eqs. (1.9) and (1.12)]. This is shown in Fig. 12.

The fitting parameters in this comparison are the values of c and T_0. There is an arbitrariness in choosing the ranges of T over which to fit the intermediate T prediction (1.9), and this can lead to some variation in the values of c and T_0. A reasonable set of values are $c=2.06Ja$ and $T_0=0.0058J$, are used in Fig. 12. The value of c is roughly consistent with that estimated earlier,[42] but the value of T_0 does appear to be rather small.

ACKNOWLEDGMENTS

We thank I. Affleck, K. Damle, B. Frischmuth, Y.-J. Kim, B. McCoy, G. Müller, F. Naef, B. Narozhny, G. Reiter, T. M. Rice, M. Takigawa, and M. Troyer for helpful discussions. This research was supported by NSF Grant No. DMR 96-23181.

APPENDIX A: CROSSOVER ENERGY SCALES FOR $\theta=\pi$

This appendix will derive the relationship (1.12) between the two energy scales T_0 and $\Lambda_{\overline{MS}}$ associated with the quantum O(3) nonlinear sigma model at $\theta=\pi$. This model has a flow from the high-energy fixed point at $g=0$ to the low-energy fixed point at $g=g_c$. The flows near both fixed points are marginal: $\Lambda_{\overline{MS}}$ is the energy scale characterizing the flow away from the $g=0$ fixed point, while T_0 is the scale characterizing the flow into the $g=g_c$ fixed point. These scales appear in the logarithmic corrections that appear in both the high-temperature [Eqs. (1.9) and (1.10)] and low- temperature [Eq. (1.7)] limits. A complete Bethe ansatz analysis of the flow between the two fixed points matches the two scales, and leads to the relationship (1.12).

We will perform the matching by considering various limiting regimes of the free-energy density $\mathcal{F}_Q$ of $\mathcal{Z}_Q$ as a function of T and H. This is will allow us to make an intricate series of mappings between numerous results which have appeared recently in the literature.

First, let us consider the low-T and low-H regime, where $T,H\ll T_0$. In this regime, the model is in the vicinity of the $g=g_c$ fixed point, which is the $k=1$, $SU(2)$ Wess-Zumino-Witten model. We know from Eq. (1.7) that for $H\ll T\ll T_0$, the free energy has a contribution

$$\mathcal{F}_Q=-\frac{H^2}{4\pi c}\left(1+\frac{1}{2\ln(T_0/T)}\right)+\cdots;\quad H\ll T\ll T_0. \tag{A1}$$

From this we anticipate that for $T\ll H\ll T_0$, we will have a corresponding contribution

$$\mathcal{F}_Q=-\frac{H^2}{4\pi c}\left(1+\frac{1}{2\ln(C_1T_0/H)}\right)+\cdots;\quad T\ll H\ll T_0, \tag{A2}$$

where C_1 is a universal number we would like to determine. The universality of C_1 implies that we can use any model which is in the vicinity of the $k=1$, $SU(2)$ Wess-Zumino-Witten fixed point. In particular, Lukyanov[22] has recently computed the detailed H and T dependence of the free energy of the $S=1/2$ antiferromagnetic chain with nearest-neighbor exchange which fulfills this requirement, and we can use his results to obtain C_1. In particular, from Eqs. (3.18) and (3.20) of Ref. 22 we determine that

$$T_0=\left(\frac{\pi}{2}\right)^{1/2}e^{\gamma+1/4}J \tag{A3}$$

for the nearest-neighbor $S=1/2$ antiferromagnet, and that

$$\mathcal{F}_Q=-\frac{H^2}{4\pi c}\left(1+\frac{1}{2\ln(2\pi e^{-\gamma}T_0/H)}\right)+\cdots;$$

$$H\ll T_0,\quad T=0. \tag{A4}$$

We emphasize that the result (A3) is nonuniversal, while Eq. (A4) is universal, i.e., only the latter is a property of the continuum O(3) nonlinear sigma model at $\theta=\pi$. In the result (A4) we have set $T=0$, as this is the limit in which we shall use in the following.

Let us now consider the vicinity of the $g=0$ fixed point for nonzero H at zero temperature, i.e., for $H\gg\Lambda_{\overline{MS}}\sim T_0$ at $T=0$. In this case, a renormalized perturbation theory in g can be used to determine the free-energy density, and this was carried out by Hasenfratz *et al.*[21] They obtained

$$\mathcal{F}_Q=-\frac{H^2}{4\pi c}\ln\left(\frac{H}{e^{1/2}\Lambda_{\overline{MS}}}\right)+\cdots;\quad H\gg\Lambda_{\overline{MS}},\quad T=0. \tag{A5}$$

Finally, we need to match Eqs. (A4) and (A5) by computing the $T=0$ free energy for $H\neq 0$ in both the low- and

high-field limits of the O(3) nonlinear sigma model at $\theta = \pi$. Fortunately, precisely this computation was carried out by Fateev, Onofri, and Zamolodchikov.[23] They obtained Eq. (A5) in the limit $H \gg \Lambda_{\overline{MS}}$, while the result for the opposite limit $H \ll \Lambda_{\overline{MS}}$ is in Eq. (4.97) of Ref. 23:

$$\mathcal{F}_Q = -\frac{H^2}{4\pi c}\left(1 + \frac{1}{2\ln(2\sqrt{2\pi}e^{-3/4}\Lambda_{\overline{MS}}/H)}\right) + \cdots; \quad H \ll \Lambda_{\overline{MS}}, \quad T = 0. \tag{A6}$$

Comparing Eq. (A6) with Eq. (A4), we immediately obtain Eq. (1.12).

APPENDIX B: SHORT-TIME EXPANSION: DETAILS

We start with the expression (2.2) and insert Eq. (2.4) into it and expand to first order to find

$$\mathcal{Z}_c = \int \mathcal{D}\psi\, \mathcal{D}\psi^*\, \mathcal{D}\phi\, \mathcal{D}\phi^* \exp\left(-\int dx\, \mathcal{L}\right), \tag{B1}$$

where

$$\mathcal{L} = \psi\psi^* + \frac{1}{2\xi}(\phi\psi^* + \phi^*\psi)^2 + \left|\frac{\partial\phi}{\partial x}\right|^2 + \frac{1}{2\xi}\left(\phi\frac{\partial\phi^*}{\partial x} + \phi^*\frac{\partial\phi}{\partial x}\right)^2 + m^2\phi\phi^* + \frac{m^2}{2\xi}\phi^2\phi^{*2} - \frac{1}{2a\xi}\phi\phi^*. \tag{B2}$$

Here we have dropped some additive constants and integrated by parts in places. As advertised before, the magnetic field in the z direction parametrized by m^2 adds a mass term to the action and makes the $\langle\phi\phi^*\rangle$ propagator infrared finite. The last term in the action arises from the Jacobian of the delta functionals $\delta(\mathbf{n}\cdot\mathbf{L})\,\delta(\mathbf{n}^2-1)$ in the measure. This Jacobian is infinite for a continuum system. To regularize it, we can introduce a discrete lattice in space. In that case the parameter a is the lattice constant, or equivalently the volume of the Brillouin zone:

$$\frac{1}{a} \equiv \frac{1}{L}\sum_{k\in \mathrm{BZ}} 1. \tag{B3}$$

This can be finite only in a finite-volume system, but we shall carry it through and ultimately it will cancel all ultraviolet divergences arising from unrestricted momentum sums over the $\langle\psi\psi^*\rangle$ propagator. In terms of ψ and ϕ, the $\langle\mathbf{L}(x,t)\cdot\mathbf{L}(0,0)\rangle$ is written as

$$\begin{aligned}\langle\mathbf{L}(x,t)\cdot\mathbf{L}(0,0)\rangle &= \langle\psi(x,t)\psi^*(0,0)\rangle + \text{c.c.} \\ &\quad + \frac{1}{\xi}\langle\phi(x,t)\psi^*(x,t)\phi(0,0)\psi^*(0,0)\rangle + \text{c.c.} \\ &\quad + \frac{1}{\xi}\langle\psi(x,t)\phi^*(x,t)\psi^*(0,0)\phi(0,0)\rangle + \text{c.c.}\end{aligned} \tag{B4}$$

Using Eq. (2.4) in the dynamical Eqs. (2.1), we find the following equations of motion:

$$\frac{\partial\psi}{\partial t} = i\left[\frac{\partial^2\phi}{\partial x^2} + \frac{1}{\xi}\frac{\partial}{\partial x}\left(\phi^2\frac{\partial\phi^*}{\partial x}\right)\right],$$

$$\frac{\partial\phi}{\partial t} = -i\left[\psi + \frac{1}{\xi}(\phi^2\psi^*)\right]. \tag{B5}$$

These equations differ from Eq. (2.5) in that we have absorbed a factor of $c = \xi^{1/2}$ into the definition of time so that time and distance have the same units.

To solve for $\psi(x,t)$, we make a Fourier transform in space of Eq. (B5) and convert it to an initial value problem given by

$$\frac{\partial}{\partial t}\begin{pmatrix}\psi(k,t)\\ \phi(k,t)\end{pmatrix} = \begin{pmatrix}-ik^2\phi(k,t)\\ -i\psi(k,t)\end{pmatrix} + \begin{pmatrix}A(k,t)\\ B(k,t)\end{pmatrix}. \tag{B6}$$

We have here written the nonlinearities as the inhomogeneous part of a set of first-order equations. The solution to the initial value problem is given by

$$\begin{pmatrix}\psi(k,t)\\ \phi(k,t)\end{pmatrix} = \mathcal{K}(t)\mathcal{K}^{-1}(0)\begin{pmatrix}\phi(k,0)\\ \psi(k,0)\end{pmatrix} + \mathcal{K}(t)\int_0^t d\tau\,\mathcal{K}^{-1}(\tau)\begin{pmatrix}A(k,\tau)\\ B(k,\tau)\end{pmatrix}. \tag{B7}$$

The columns of the 2×2 matrix $\mathcal{K}(t)$ is made up of the two linearly independent solution vectors of the homogeneous problem:

$$\mathcal{K}(t) = \begin{pmatrix}ke^{-ikt} & -ke^{ikt}\\ e^{-ikt} & e^{ikt}\end{pmatrix} \tag{B8}$$

Armed with this, we can solve for the fields in terms of the initial conditions and iterate the solution to go to higher orders by plugging the solution back in A and B. Also calculations simplify very much if we work out everything back in real space. So at last we write down the final iterative form from which the entire perturbation series can be generated:

$$\begin{aligned}\psi(x,t) &= \frac{1}{2}[\psi(x+t,0) + \psi(x-t,0)] + \frac{i}{2}\frac{\partial}{\partial x}[\phi(x+t,0) - \phi(x-t,0)] + \frac{1}{2}\int_0^t d\tau\int dx'[\delta(x-x'+t-\tau) \\ &\quad + \delta(x-x'-t+\tau)]A(x',\tau) + \frac{i}{2}\int_0^t d\tau\int dx' \\ &\quad \times[\delta(x-x'+t-\tau) - \delta(x-x'-t+\tau)] \\ &\quad \times\frac{\partial}{\partial x'}B(x',\tau),\end{aligned} \tag{B9}$$

$$\phi(x,t)=\frac{1}{2}[\phi(x+t,0)+\phi(x-t,0)]-\frac{i}{2}\int dx'[\theta(x-x'+t)-\theta(x-x'-t)]\psi(x',0)+\frac{1}{2}\int_0^t d\tau\int dx'\times[\delta(x-x'+t-\tau)+\delta(x-x'-t+\tau)]B(x',\tau)-\frac{i}{2}\int_0^t d\tau\int dx'[\theta(x-x'+t-\tau)-\theta(x-x'-t+\tau)]A(x',\tau) \tag{B10}$$

To simplify notation let us denote the zero-order solutions for the fields as $\psi^{(0)}(x,t)$ and $\phi^{(0)}(x,t)$:

$$\psi^{(0)}(x,t)=\frac{1}{2}[\psi(x+t,0)+\psi(x-t,0)]+\frac{i}{2}\frac{\partial}{\partial x}[\phi(x+t,0)-\phi(x-t,0)],$$

$$\phi^{(0)}(x,t)=\frac{1}{2}[\phi(x+t,0)+\phi(x-t,0)]-\frac{i}{2}\int dx'[\theta(x-x'+t)-\theta(x-x'-t)]\psi(x',0). \tag{B11}$$

Now we can proceed to evaluate each of the correlation functions in Eq. (B4). As an example let us look at $\langle\psi(x,t)\psi^*(0,0)\rangle$. The correlations to zero order are

$$\langle\psi^{(0)}(x,t)\psi^{(0)*}(0,0)\rangle=\frac{1}{2}[\delta(x+t)+\delta(x-t)],$$

$$\langle\phi^{(0)}(x,t)\phi^{(0)*}(0,0)\rangle=\frac{1}{4m}(e^{-m|x+t|}+e^{-m|x-t|}),$$

$$\langle\phi^{(0)}(x,t)\psi^{(0)*}(0,0)\rangle=\frac{i}{2}[\theta(x+t)-\theta(x-t)]. \tag{B12}$$

To compute the one-loop correlation $\langle\psi(x,t)\psi^*(0,0)\rangle$, we write down

$$\langle\psi(x,t)\psi^*(0,0)\rangle=\langle\psi^{(0)}(x,t)\psi^{(0)*}(0,0)\rangle+\frac{1}{2}\int_0^t d\tau\int dx'[\delta(x-x'+t-\tau)+\delta(x-x'-t+\tau)]\times\frac{1}{\xi}\frac{\partial}{\partial x'}\left\langle\phi^2(x',\tau)\frac{\partial\phi^*(x',\tau)}{\partial x'}\psi^{(0)*}(0,0)\right\rangle+\frac{i}{2}\int_0^t d\tau\int dx'[\delta(x-x'+t-\tau)-\delta(x-x'-t+\tau)]\times\frac{\partial}{\partial x'}\left\langle-\frac{i}{\xi}\phi^2(x',\tau)\psi^*(x',\tau)\psi^{(0)*}(0,0)\right\rangle. \tag{B13}$$

On the second and third terms of the RHS, we can replace $\phi(\psi)$ by $\phi^{(0)}$ $(\psi^{(0)})$ since it is already first order in $1/\xi$. Now all the correlation functions on the RHS are expressed in terms of correlation functions at time $t=0$. So we evaluate them using the partition function (B1). Other correlations can be evaluated in the same manner. So we shall only write down the final answers here:

$$\langle\psi(x,t)\psi^*(0,0)\rangle=\frac{1}{2}[\delta(x+t)+\delta(x-t)]\left(1-\frac{1}{2m\xi}\right), \tag{B14}$$

$$\langle\phi(x,t)\psi^*(x,t)\phi(0,0)\psi^*(0,0)\rangle=\frac{1}{4\xi}[\theta(x+t)-\theta(x-t)], \tag{B15}$$

$$\langle\psi(x,t)\phi^*(x,t)\psi^*(0,0)\phi(0,0)\rangle=\frac{1}{8m\xi}[\delta(x+t)+\delta(x-t)](1+e^{-2mt}). \tag{B16}$$

Adding them all and taking the limit $m\to 0$ leads to the expression quoted in Eq. (2.6). Note that all terms which diverge as $m\to 0$, cancel each other only when we evaluate the O(3) invariant correlation $\langle\mathbf{L}(x,t)\cdot\mathbf{L}(0,0)\rangle$.

APPENDIX C: EVALUATION OF THE ONE-PARTICLE DISTRIBUTION FUNCTION

Let us start with Eq. (4.8). Following Jepsen's notation we write

$$P(y,t)=\sum_{k\neq 0}\langle\delta(y-x_k-v_kt)A_{0k}(t)\rangle+\langle\delta(y-v_0t)A_{00}(t)\rangle=\frac{1}{N}\sum_u\frac{N-1}{L}e^{-iju}\int_0^L dx_k\int_{-\infty}^{\infty}dv_k\,g(v_k)\times Q(u,x_k+v_kt,v_k)\times\left[\frac{1}{L}\int_0^L dx_h R[u,x_k+v_kt-x_h]\right]^{N-2}+\frac{1}{N}e^{-iju}\int_{-\infty}^{\infty}dv_0\,g(v_0)\delta(y-v_0t)\times\left[\frac{1}{L}\int_0^L dx_h\,R[u,x_0+v_0t-x_h]\right]^{N-1}, \tag{C1}$$

with the definitions that

$$g(v_k)=\frac{1}{2}[\delta(v_k-c)+\delta(v_k+c)],$$

$$Q(u,x_k+v_kt,v_k)=\int_{-\infty}^{+\infty}dv_0\,g(v_0)\,\delta(y-x_k-v_kt)\times S(u,x_k+v_kt-v_0t)=\frac{1}{2}\,\delta(y-x_k-v_kt)\times[S(u,y-ct)+S(u,y+ct)],$$

$$R[u,x_k+v_kt-x_h]=\int_{-\infty}^{+\infty}dv_h\,g(v_h)S(u,x_k+v_kt-x_h-v_ht). \tag{C2}$$

The second term in the RHS of Eq. (C1) clearly represents the probability that the zero particle stays in the zero trajectory at time t, while the first term represents the probability that it has been scattered to another trajectory. The second term can be easily simplified using the definitions given above and in Eq. (4.5). It is

$$[\delta(y+ct)+\delta(y-ct)]P^{(1)}(t)=\delta(y-ct)\frac{1}{2N}\sum_u\left\{\frac{1}{2}\left[1+e^{ipu}\left(1+\frac{2ct-pL}{L}\times(e^{iu}-1)\right)\right]\right\}^{N-1}+\delta(y+ct)\frac{1}{2N}\sum_u\times\left\{\frac{1}{2}\left[1+e^{-ipu}\left(1+\frac{2ct-pL}{L}(e^{-iu}-1)\right)\right]\right\}^{N-1}. \tag{C3}$$

Here p is defined so that

$$0<2ct-pL<L. \tag{C4}$$

$P^{(1)}(t)$ cannot be evaluated in a closed analytic form. But we have evaluated it numerically for fixed values of N and L. $P^{(1)}(t)$ has been plotted in Fig. 9 for $N=50,L=1,c=\pm1$. As mentioned before, the peaks at times $\mathcal{T},2\mathcal{T},3\mathcal{T},\ldots$, are due to the exact recurrence of some configurations. We plot this function again for $N=50$ and $51,L=1,c=\pm1$ in Fig. 10. Note that the peaks at times $\mathcal{T},2\mathcal{T}\ldots$, disappear.

The first term will be handled in a manner similar to above. For simplicity we shall evaluate only the autocorrelation part. To do this, we set $y=nL$ where n is an integer.

$$P^{(2)}(t)=\sum_{k\neq0}\langle\delta(x_k+v_kt-nL)A_{0k}(t)\rangle. \tag{C5}$$

Using previous definitions we find that

$$P^{(2)}(t)=\frac{1}{4N}\sum_u\frac{N-1}{L}[\theta(nL-ct)-\theta(nL-ct-L)+\theta(nL+ct)-\theta(nL+ct-L)]\times(S[u,nL+ct]+S[u,nL-ct])\times\left(\int_0^L\frac{dx}{2L}(S[u,nL-x-ct]+S[u,nL-x+ct])\right)^{N-2}. \tag{C6}$$

Here it will be convenient to define an integer p as before such that

$$0<ct-pL<L. \tag{C7}$$

Carrying out the integrals above we get

$$P^{(2)}(t)=\frac{1}{4N}\sum_u\frac{N-1}{L}(e^{-iu}+e^{2ipu})\frac{1}{2^{N-2}}\times\left[\frac{L-(ct-pL)}{L}(1+e^{2ipu})+\frac{ct-pL}{L}\times(e^{-iu}+e^{i(2p+1)u})\right]^{N-2}+\text{c.c.} \tag{C8}$$

The above function $P^{(2)}(t)$ has been plotted in Fig. 11.

[1] M. Takigawa, T. Asano, Y. Ajiro, M. Mekata, and Y. J. Uemura, Phys. Rev. Lett. **76**, 2173 (1996).
[2] M. Takigawa, O. A. Starykh, A. W. Sandvik, and R. R. P. Singh, Phys. Rev. B **56**, 13 681 (1997).
[3] M. Takigawa, N. Motoyama, H. Eisaki, and S. Uchida, Phys. Rev. B **55**, 14 129 (1997).
[4] K. Damle and S. Sachdev, Phys. Rev. B **57**, 8307 (1998).
[5] H. Schulz, Phys. Rev. B **34**, 6372 (1986).
[6] S. Sachdev, Phys. Rev. B **50**, 13 006 (1994).
[7] O. A. Starykh, R. R. P. Singh, and A. W. Sandvik, Phys. Rev. Lett. **78**, 539 (1997).
[8] O. A. Starykh, A. W. Sandvik, and R. R. P. Singh, Phys. Rev. B **55**, 14 953 (1997).
[9] F. B. McLean and M. Blume, Phys. Rev. B **7**, 1149 (1973).
[10] G. Reiter and A. Sjölander, J. Phys. C **13**, 3027 (1980).
[11] N. Elstner, A. Sokol, R. R. P. Singh, M. Greven, and R. J. Birgeneau, Phys. Rev. Lett. **75**, 938 (1995).
[12] O. F. Syljuåsen, S. Chakravarty, and M. Greven, Phys. Rev. Lett. **78**, 4115 (1997).
[13] I. Affleck and F. D. M. Haldane, Phys. Rev. B **36**, 5291 (19xx).
[14] A. M. Tsvelik, Zh. Éksp. Teor. Fiz. **93**, 385 (1987) [Sov. Phys. JETP **66**, 221 (1987)].
[15] M. Troyer, H. Tsunetsugu, and T. M. Rice, Phys. Rev. B **53**, 251 (1996).
[16] S. Chakravarty, Phys. Rev. Lett. **77**, 4446 (1996).
[17] Y. J. Kim, M. Greven, U.-J. Wiese, and R.J. Birgeneau, Eur. Phys. J. B **4**, 291 (1998).
[18] S. Eggert, I. Affleck, and M. Takahashi, Phys. Rev. Lett. **73**, 332 (1994).
[19] K. Nomura, Phys. Rev. B **48**, 16 814 (1993).
[20] K. Nomura and M. Yamada, Phys. Rev. B **43**, 8217 (1991).
[21] P. Hasenfratz, M. Maggiore, and F. Niedermayer, Phys. Lett. B **245**, 522 (1990).
[22] S. Lukyanov, Nucl. Phys. B **522**, 533 (1998).

[23] V. A. Fateev, E. Onofri, and Al. B. Zamolodchikov, Nucl. Phys. B **406**, 521 (1993).
[24] L. D. Faddeev and L. A. Takhtajan, *Hamiltonian Methods in the Theory of Solitons* (Springer-Verlag, Heidelberg, 1987).
[25] D. Forster, *Hydrodynamic Fluctuations, Broken Symmetry, and Correlation Functions* (Benjamin/Cummings, Reading, MA, 1975).
[26] U. Wolff, Phys. Rev. Lett. **62**, 361 (1989).
[27] N. Srivastava, J.-M. Liu, V. S. Viswanath, and G. Müller, J. Appl. Phys. **75**, 6751 (1994).
[28] O. F. de Alcantara Bonfim and G. Reiter, Phys. Rev. Lett. **69**, 367 (1992); **70**, 249 (1993).
[29] A. V. Chubukov, S. Sachdev, and J. Ye, Phys. Rev. B **49**, 11 919 (1994).
[30] Th. Jolicoeur and O. Golinelli, Phys. Rev. B **50**, 9265 (1994).
[31] B. N. Narozhny, Phys. Rev. B **54**, 3311 (1996).
[32] X. Zotos, F. Naef, and P. Prelovsek, Phys. Rev. B **55**, 11 029 (1997); F. Naef and X. Zotos, J. Phys.: Condens. Matter **10**, L183 (1998).
[33] B. N. Narozhny, A. J. Millis, and N. Andrei, Phys. Rev. B **58**, R2921 (1998).
[34] K. Fabricius and B. M. McCoy, Phys. Rev. B **57**, 8340 (1998).
[35] X. Zotos, Phys. Rev. Lett. **82**, 1764 (1999).
[36] D. W. Jepsen, J. Math. Phys. **6**, 405 (1965).
[37] J. L. Lebowitz and J. K. Percus, Phys. Rev. **155**, 122 (1967).
[38] R. J. Birgeneau, R. Dingle, M. T. Hutchings, G. Shirane, and S. L. Holt, Phys. Rev. Lett. **26**, 718 (1971); M. T. Hutchings, G. Shirane, R. J. Birgeneau, and S. L. Holt, Phys. Rev. B **5**, 1999 (1972).
[39] M. T. Hutchings and C. G. Windsor, J. Phys. C **10**, 313 (1977).
[40] G. E. Granroth, M. W. Meisel, M. Chaparala, T. Jolicoeur, B. H. Ward, and D. R. Talham, Phys. Rev. Lett. **77**, 1616 (1996).
[41] S. Itoh, Y. Endoh, K. Kakurai, and H. Tanaki, Phys. Rev. Lett. **74**, 2375 (1995).
[42] B. Frischmuth, S. Haas, G. Sierra, and T. M. Rice, Phys. Rev. B **55**, R3340 (1997); B. Frischmuth, B. Ammon, and M. Troyer, Phys. Rev. B **54**, R3714 (1996).